A synthesis of the environmental response of the North and South Atlantic Sub-Tropical Gyres during two decades of AMT

Jim Aiken[1], Robert J. W. Brewin[1,2,*], Francois Dufois[3], Luca Polimene[1], Nick Hardman-Mountford[3] , Thomas Jackson[1], Ben Loveday[1], Silvana Mallor Hoya[1,4], Giorgio Dall'Olmo[1,2], John Stephens[1] & Takafumi Hirata[5]

[1]Plymouth Marine Laboratory (PML), Prospect Place, the Hoe, PL1 3DH, Plymouth, UK

[2]National Centre for Earth Observation, PML, Prospect Place, the Hoe, PL1 3DH, Plymouth, UK

[3]CSIRO Oceans and Atmosphere Flagship, Wembley, Western Australia, Australia

[4]NERC Earth Observation Data Acquisition and Analysis Service, PML, Prospect Place, the Hoe, PL1 3DH, Plymouth, UK

[5]Faculty of Environmental Earth Science, Hokkaido University, N10W5 Sapporo,

Hokkaido 060-0810, Japan

*E-mail: robr@pml.ac.uk

Abstract

Anthropogenically-induced global warming is expected to decrease primary productivity in the subtropical oceans by strengthening stratification of the water column and reducing the flux of nutrients from deep-waters to the sunlit surface layers. Identification of such changes is hindered by a paucity of long-term, spatially-resolved, biological time-series data at the basin scale. This paper exploits Atlantic Meridional Transect (AMT) data on physical and biogeochemical properties (1995-2014) in synergy with a wide range of remote-sensing (RS) observations from ocean colour, Sea Surface Temperature (SST), Sea Surface Salinity (SSS) and altimetry (surface currents), combined with different modelling approaches (both empirical and a coupled 1-D Ecosystem model), to produce a synthesis of the seasonal functioning of the North and South Atlantic Sub-Tropical Gyres (STGs), and assess their response to longer-term changes in climate. We explore definitive characteristics of the STGs using data of physical (SST, SSS and peripheral current systems) and biogeochemical variables (chlorophyll and nitrate), with inherent criteria (permanent thermal stratification and oligotrophy), and define the gyre boundary from a sharp gradient in these physical and biogeochemical properties. From RS data, the seasonal cycles for the period 1998-2012 show significant relationships between physical properties (SST and PAR) and gyre area. In contrast to expectations, the surface layer chlorophyll concentration from RS data (CHL) shows an upward trend for the mean values in both subtropical gyres. Furthermore, trends in physical properties (SST, PAR, gyre area) differ between the North and South STGs, suggesting the processes responsible for an upward trend in CHL may vary between gyres. There are significant anomalies in CHL and SST that are associated with El Niño events. These conclusions are drawn cautiously considering the short length of the time-series (1998-2012), emphasising the need to sustain spatially-extensive surveys such as AMT and integrate such observations with models, autonomous observations and RS data, to help address fundamental questions about how our planet is responding to climate change. A small number of dedicated AMT cruises in the keystone months of January and July would complement our understanding of seasonal cycles in the STGs.

Key words: Atlantic Meridional Transect, oligotrophic, subtropical gyres, *in situ*, remote-sensing, modelling, chlorophyll, phytoplankton

1. Introduction

1.1 Global warming

The ocean and atmosphere are tightly coupled in the Earth's climate system. The oceans absorb anthropogenically produced CO_2 (Le Quéré et al. 2014) and heat produced by global warming (Bindoff et al. 2007). Data from the International Panel on Climate Change (IPCC) report and International Geosphere-Biosphere Programme (IGBP) show a steady rise in the Earth's temperature from the 1880s to present, in line with increases in atmospheric CO_2 concentration, with considerable inter-annual to decadal variability and recently (1996-2014), periods of little or no warming (Pörtner et al. 2014; Table 1 lists Acronyms and Abbreviations). Ocean biogeochemistry has been impacted by climate change with rising sea surface temperature (SST) and acidification (Pörtner et al. 2014; Kitidis et al. Submitted this issue). Changing climate patterns, such as increased hurricane intensity and longevity, are linked to high SST (>25°C) in the tropical oceans (Goldenberg et al. 2001); increased evaporation leads to higher energy and turbulence in the atmosphere and increased frequency of tropical storms. There is evidence that, in a warmer world with warmer oceans, events such as El Niño (an irregular large-scale ocean-atmosphere climate interaction linked with periodic ocean warming) are more frequent (Wara et al. 2005).

The oceans are ~72% of the Earth's surface and the Sub-Tropical Gyres (STGs) and tropical equatorial regions (TER) consist of ~50% of the Earth surface. The ocean heat capacity (OHC) for the upper 700 m (and 300m) approximately tracks the rise in the Earth's temperature 1948-2008, for the World Ocean, Atlantic, Pacific and Indian Oceans and their sub-basins (Levitus et al, 2000, 2001, 2005). In recent decades (1995-present) a hiatus in rising OHC for the upper 700 m has been observed despite increased atmospheric warming, which has been attributed to the deep ocean (>700m) taking up a greater proportion of the OHC (Meehl et al. 2011; Tollefson 2014). Figure 1 highlights global temperature observations and atmospheric CO_2 concentration from 1978 to present, coincident with the era of remote sensing (RS) observations of ocean colour and SST, and the concurrent period of Atlantic Meridional Transect (AMT) cruises.

1.2 The Atlantic Meridional Transect (AMT)

The Atlantic Meridional Transect (AMT) programme consists of a time-series of oceanographic stations along a 13,500km north-south transect (50°N-50°S) in the Atlantic Ocean (Aiken et al. 2000; Robinson et al. 2006). The AMT was created from two NERC 'PRIME' projects, 'Holistic Biological Oceanography' (Aiken, Holligan & Watson) and 'Optical characterisation of Zooplankton' (Robins, Harris & Pilgrim). Together they exploited the passage of the RRS James Clark Ross (JCR) from the United Kingdom to the Falkland Islands (Phase 1 1995-2000), southward in September, returning northward the following April or May after the Antarctic summer. Project objectives were to integrate shipboard measurements of physical and biogeochemical variables (e.g. SST, salinity (SAL), Chlorophyll (Chla), and nitrate (NO_3)), and air-sea exchange of bio-gases (e.g. CO_2), with RS data (e.g. surface chlorophyll from RS (CHL) and SST) and modelling, to test and refine hypotheses on the impact of anthropogenically-forced environmental change on ocean ecosystems and air-sea interactions in the Earth Climate System (Aiken et al. 2000).

Subsequent phases of the AMT cruises followed Phase 1, but with only one cruise per year (September-November), including: Phase 2 from 2002-2005; and Phase 3 and 4, from 2008-present. Figure 2 shows the annual and seasonal coverage of AMT-1 through to AMT-25 (1995-2015). Cruises lack detailed seasonal coverage, but have depth resolution captured in >1500 CTD casts (typically to 300m, some 1000 to 5000m); >1000 bio-optical profiles; and data for co-related biogeochemical variables and process rates (productivity, zooplankton biomass, air-sea exchange of CO_2 and other biogenic gases), as described in detail in the online cruise reports (http://www.amt-uk.org/Cruises). AMT is one of a few spatially-extensive surveys acquiring multiple datasets of oceanographic variables over two decades using state of the art instrumentations and methodologies.

1.3 Remote sensing (RS)

The first AMT cruise (AMT-1) was scheduled to coincide with the delayed launch of the SeaWiFS (NASA) ocean-colour sensor in September 1995. However, the launch was delayed to September 1997, coinciding with the start of AMT-5. In the interim the OCTS ocean-colour sensor (NASDA, Japan) provided partial coverage for AMT-3 and good coverage for AMT-4 before mal-functioning. SeaWiFS provided coverage from 1997 until 2010, when the instrument sensitivity diminished but ocean-colour remote-sensing coverage was maintained with MODIS (2002-present) and MERIS (2002-2012) sensors, and more recently VIIRS (2012-present). Ocean-colour sensors CZCS (1978-86), OCTS (1996-97), SeaWiFS, MERIS and MODIS-Aqua, have provided time-series CHL, monitoring changes of ocean biogeochemistry that have led to significant advances in our understanding of marine ecosystems (McClain et al. 2009). The merging of ocean-colour data sets within the Ocean Colour Climate Change Initiative (OC-CCI) project (Müller et al. 2015a; 2015b; Brewin et al. 2015) is a key attribute utilised here, and provides enhanced coverage of ocean colour data in the Atlantic Ocean.

Successive satellites carrying AVHRR sensors for SST (NOAA; since 1981) have been supplemented by ATSR and AATSR (ESA since 1991) to produce a long-term integrated data set of SST that continues to the present. Satellite data shows rising SST to the mid 90’s with a noticeable hiatus over recent two decades (Merchant et al. 2012). Additionally, RS altimetry products such as sea-surface height (SSH) have been available since 1993, allowing the calculation of geostrophic velocities that offer a synoptic picture of the stronger geostrophic currents that constrain the boundaries of the STGs, and the lower-velocity currents within (McClain et al. 2004). Sea Surface Salinity (SSS) from SMOS have provided novel insight into surface salinity patterns, but only for brief periods (Font et al. 2010).

Satellite RS observations of several ocean and atmosphere variables (including: SST, CHL, photosynthetically available radiation (PAR), SSS and geostrophic currents) provide data at daily, annual and decadal time periods. Though lacking information on vertical structure, RS data provides detailed seasonal coverage not available on AMT cruises.

1.4 Ecosystem Modelling

Ecosystem modelling techniques have been used to understanding sub-surface properties not observable from RS data. This has included establishing empirical links between surface-layer and sub-surface properties (Morel & Berthon 1989; Uitz et al. 2006) and developing coupled physical-biogeochemcial ecosystem models (Holt et al. 2014). Hardman-Mountford et al. (2013) used the 1D European Regional Sea Ecosystem Model (ERSEM) to simulate coupled physical-ecosystem processes at the centre of the South Atlantic Gyre (SAG), capturing all the main features of this oligotrophic gyre, including a surface chlorophyll maximum in mid-winter. Their results suggest that the total water column chlorophyll (vertically integrated Chla) is relatively quasi-constant over a season, but can change with inter-annual fluctuations of PAR, which may respond to anthropogenic changes of atmospheric transparency, and effects of global warming, such as increased evaporation, water vapour and cloudiness. Ecosystem models have the capability to integrate and extrapolate *in situ* data and RS observations to decadal scales, pre-AMT and into the future.

1.5 Sub-Tropical Gyres (STGs)

The oligotrophic Sub-Tropical Gyres (STGs), and the Tropical Equatorial Region (TER), also oligotrophic, cover approximately 50% of the Earth's surface. The North Atlantic Gyre (NAG) and South Atlantic Gyre (SAG) are each ~5% of the Earth's surface area. The unique biogeochemistry of the STGs results from permanent thermal stratification (all year, every year) and a quasi-isothermal surface mixed layer (SML, 50m to >150m, nutrient depleted and oligotrophic). Below the SML there is a thermocline that supports a deep chlorophyll maximum (DCM) fertilised by nutrients from deeper waters; both SML and DCM have variable seasonal characteristics (McClain et al. 2004). The physical structure leads to light driven biological production in the DCM, which controls nutrient fluxes, with maximum production and Chla in the DCM occurring at mid-summer when solar insolation (SI) is greatest and least when light is lowest in mid-winter (Hardman-Mountford et al. 2013). Conversely production and Chla in the surface layer (CHL) are least when SI is greatest at mid-summer and greatest at mid-winter when SI is least (McClain et al. 2004). Thus, surface Chla and SI are approximately six months out of phase. The winter surface Chla maximum partly results from lower SI (less stratification), less production in the DCM and less usage of nutrients therein, allowing upward nutrient diffusion to fertilise the mixed layer (this has been termed the 'Light Effect', see Taylor, Harris & Aiken, 1986). A deepening of the mixed layer by convectional cooling in winter may also erode the thermocline, nutracline and DCM, releasing nutrients to fertilise the surface layer (Signorini et al. 2015). Contraction of the gyres in winter may also add nutrients at the gyre edges, impacting seasonal cycles in Chla.

The spatial area of the STG has been quantified previously using surface chlorophyll concentrations (CHL). Research by McClain et al (2004), Polovina et al (2008), and Signorini et al (2015) have chosen a concentration of 0.07 mg m^{-3} Chla, to define the gyre edge. This value encompasses only the core of the gyres. Aiken et al. (2000, 2009) suggested values of 0.15 to 0.2 mg m^{-3} (see data on CHL and accessory pigments in Figs. 34 and 35 of Aiken et al. (2000), and a comparison of CHL by HPLC and from SeaWiFS in Fig 36 of Aiken et al. (2000) and in Fig. 2 of Aiken et al (2009)). Hirata et al, (2008) and Brewin et al. (2010) show the switch from pico-plankton dominance (pro-chlorophytes and pico-eukaryotes) occurs at around >0.15-0.2 g m^{-3}, this could indicate that pico-eukaryotes still dominate at higher nutrient concentrations at the gyre edge. It is important to construct a robust definition of the gyres, to facilitate our understanding of how the gyres may be changing with climate change.

In this paper, we combine *in situ* data from AMT with RS datasets and ecosystem modelling, to develop a holistic understanding of NAG and SAG processes, and their spatial (both horizontal and vertical), seasonal and inter-annual variability. We develop a robust definition of the gyre area, based on their distinct physical and biological properties. Finally, we explore changes in the physics and biogeochemistry of the gyres over the past two decades.

2. Methods

2.1 AMT sampling strategy

AMT cruises transect the North and South Atlantic from nominally 50°N to 50°S (~13,500 km). Cruises have been either: south-bound from the UK (September, October and November) sampling the NAG during the boreal fall and transecting the SAG during the austral spring (denoted BFAS cruises); or north bound from either the Falkland Islands or Cape Town (typically April and May), sampling the South Atlantic in the austral fall and the North Atlantic in spring (denoted AFBS cruises). In general, seasonal coverage is poor (see Fig 2). There have been no AMT cruises in mid-winter or mid-summer (December, January, February, March, July and August), with partial sampling in April (5 cruises), May (7 cruises) and June (4 cruises), and most frequent sampling in September and October (15 cruises) and November (8 cruises). BFAS cruises have coincided with the maximum SST in the NAG (September) and the minimum SST in the SAG (September and October). AFBS cruises have occurred a few weeks after maximum SST in the SAG and minimum SST in the NAG (April and May). Between AMT phases there have also been gaps in sampling (e.g. 2001, 2002, 2006 and 2007, see Fig. 2). With only 12.5% of days sampled between 1995 and 2014, synergistically combining AMT data with other datasets capable of sampling at finer temporal scales (such as RS data and modelling) is crucial to understanding the Atlantic ecosystem.

Figure 3 shows tracks for six AMT cruises (two from each phase) overlaid on CHL composites from contemporary RS data processed by the National Earth Observation Data Acquisition and Analysis Service (NEODAAS), with AMT-4 CHL data from the OCTS sensor and other cruises using OC-CCI CHL data (see section 2.3 below for details on the RS data). In phase 1 (Fig. 3a and 3b, AMT-4 and AMT-5) there was limited sampling in the NAG, with cruise tracks avoiding the centre of the gyres to sample the high CHL zone of the NW African Upwelling (~20°N to ~10°N). The SAG was transected from ~8°S to ~30°S in Phase 1, exiting at the western edge of the gyre close to Brazil. The north-bound cruise tracks in Phase 1 were similar but in reverse, except for AMT-6 which departed from Cape Town with a course through the Benguela Upwelling. In general, Phase 1 only partially sampled the NAG and SAG. In Phases 2 and 3, the cruise tracks transected the centres of both gyres (Fig. 3c-3f, AMT-14 through to AMT-22): along 35°W or 40°W in the NAG, crossing the pole-ward edge at ~40°N and the equatorial edge at ~15°N; along the 25°W meridian in the SAG, crossing the equatorial edge at ~5°S and the pole-ward at ~33°S. For further information on the AMT sampling strategy, refer to cruise reports on the AMT website (http://www.amt-uk.org/Cruises). Many cruise reports contain along track and *in situ* data from station casts. Quality assured data are held by the British Oceanographic Data Centre (BODC: see http://www.bodc.ac.uk/).

<u>2.1 AMT data</u>

To illustrate changes in surface biological and physical properties along a typical AMT transect, AMT-22 along-track *in situ* data for SST, SSS and CHL were utilised, measured from pumped surface-layer water at a nominal depth of 5 m, using conductivity and temperature sensors, and a fluorometer calibrated with discrete water samples following Welschmeyer (1994). The surface CHL data from a fluorometer is often 'noisy' due to air bubbles in the water stream when the vessel is at high speed between stations, or erratic due to bio-fouling of the flow-through cell. Therefore, in addition, discrete water samples (2-4 litres) were collected along the AMT-22 transect from the underway flow-through system. The water samples were filtered onto Whatman GF/F filters (~0.7µm) and stored in liquid nitrogen. Phytoplankton pigments were determined after the cruise in the laboratory using High Performance Liquid Chromatography (HPLC) analysis. CHL was determined by summing the contributions of monovinyl chlorophyll-a, divinyl chlorophyll-a and chlorophyllide-a. For AMT-22, CHL was also estimated from an ACS attached to the ship's flow-through system, following the methods of Slade et al. (2010), as described in Dall'Olmo et al. (2012) and Brewin et al. (2016), with ACS CHL estimates averaged over a 20 minute period centred on the time of the discrete HPLC water samples.

To illustrate vertical sections in biological, chemical and physical properties along a typical AMT transect, we made use of plots of vertical sections of nitrate, Chla, temperature and salinity for AMT-14 and AMT-17, extracted from AMT cruise reports. These were based on bottle and CTD data from the pre-dawn, late morning and dusk stations, measuring temperature, salinity, density, Chla and nitrate. Uncertainties can arise from the contouring (gridding) of station data. The transit time between pre-dawn and mid-day stations was typically ~4 h (~80 km), with the pre-dawn station next day ~18h later (~320 km); though occasionally there was a mid-afternoon station ~2 h after mid-day (~40 km). On both cruises concentrations of nitrate were determined using the Bran+Luebbe Autoanalyser and Liquid Waveguide Capillary Cell methods, and concentrations of Chla were determined from the CTD fluorometer, calibrated against discrete measurements for water bottle samples following Welschmeyer (1994). For further details on methods used for *in situ* data collection, the reader is referred to AMT-14, AMT-17 and AMT-22 cruise reports, available through the Atlantic Meridional Transect website (http://www.amt-uk.org/Cruises).

2.3 Remote Sensing Data (RS)

In this study we use several methods for oceanographic satellite remote sensing (RS), each occupying different wavelengths of the electromagnetic spectrum, including both passive and active sensors, and covering: visible radiometry (ocean-colour); infra-red radiometry (SST); microwave radiometry (SSS); and altimetry (geostrophic currents).

For ocean-colour, we mainly use CHL derived from the OC-CCI project (v1.0 dataset). The OC-CCI focuses on creating a consistent, error-characterised time-series of ocean-colour products, for use in climate-change studies (Muller et al. 2015a; 2015b; Brewin et al. 2015). The dataset consists of a time-series (1997-2012) of merged and bias-corrected MERIS, MODIS-Aqua and SeaWiFS data, at 4km-by-4km resolution. Satellite data from these three sensors show good temporal consistency in monthly products at seasonal and inter-annual scales (Brewin et al., 2014). Monthly CHL composites from the period 1997-2012 were used (available at http://www.oceancolour.org/), together with monthly climatology CHL data, derived from averaging each month in the time-series. For further information on OC-CCI processing, extensive documentation can be found on the ESA OC-CCI website http://www.esa-oceancolour-cci.org/. We also made use of monthly ocean-colour CHL data pre-1997, derived from the Japanese OCTS sensor and processed by NEODAAS, and monthly PAR products from SeaWiFS (9km-by-9km resolution) downloaded from the NASA ocean-colour website (http://oceancolor.gsfc.nasa.gov/).

For infra-red radiometry, we used global monthly SST data from NOAA OISST V2 (http://www.esrl.noaa.gov/psd/data/gridded/data.noaa.oisst.v2.html). For microwave radiometry, we used SSS data derived from the ESA Soil Moisture Ocean Salinity (SMOS) Earth Explorer mission. SMOS works at microwave wavebands and is capable of picking up faint microwave emissions from ocean salinity. Monthly climatology data on SSS from SMOS were obtained via http://www.smos-bec.icm.csic.es for the period 2010 to 2013. For altimetry, we analysed version5 of the SSALTO/DUACS merged, delayed-time, mean absolute dynamic topography (MADT) and geostrophic velocity products, sourced from the Archiving, Validation and Interpretation of Satellite Oceanographic Data (AVISO) website http://www.aviso.oceanobs.com/.

2.4 Ecosystem modelling

To aid our interpretation of seasonal and vertical variability in the NAG and SAG we used two different modelling approaches. Brewin et al. (Submitted this issue) developed an algorithm, adapted from the work of Platt and Sathyendranath (1988) and Uitz et al (2006) to estimate the vertical profile of chlorophyll biomass using a shifted Gaussian curve model. The approach estimates the vertical chlorophyll profile as a function of CHL estimated from RS, and was parameterised using HPLC pigment data collected on AMT transect cruises (see Brewin et al. Submitted, for further details). We used the model to illustrate seasonal changes in the ratio of chlorophyll at the DCM relative to that at the surface, and how this ratio changes with variations in PAR and mixed-layer depth (extracted from monthly climatological data; see de Boyer Montégut et al. 2004).

In addition to the empirical approach, we used recent simulations of seasonal cycles in chlorophyll and physical variables from a mechanistic 1D coupled ERSEM–GOTM model (where GOTM refers to the General Ocean Turbulence Model) designed to simulate biogeochemical processes at the centre of the SAG (Hardman-Mountford et al. 2013). ERSEM is a biomass and functional group-based biogeochemical and ecosystem model describing nutrient and carbon cycling within the lower trophic levels of the marine ecosystem (up to mesozooplankton, see Blackford et al. 2004 and Polimene et al. 2012). GOTM is a one-dimensional water column model which dynamically simulates the evolution of temperature, density and vertical mixing (Burchard et al. 1999). Hardman-Mountford et al. (2013) forced the 1D coupled ERSEM–GOTM models with physical data at the centre of the SAG (18.53°S and 25.1°W) using local environmental variables (ECWMF) and assimilating the vertical temperature structure. The resulting simulations are used here to understand seasonal cycles in chlorophyll at the surface and DCM, which are not available from AMT or RS data. For further details on the model description and set-up used, the reader is referred to Hardman-Mountford et al. (2013).

3. Results and Discussion

3.1 Properties, seasonal characteristics and definition of the gyres.

The gyres constitute a large fraction of the global ocean, yet many of their characteristic properties are not well known. The boundaries of the STGs are ill-defined, constrained by variable surface currents that enclose large relatively static water masses (Tomczak & Godfrey, 1994; see also Fig. 1 of Aiken et al, 2000). These regions are permanently thermally stratified, with low inorganic nutrients and low biomass in the surface layer, i.e. oligotrophic. The RS CHL data (Fig. 3) show the STGs are quasi-ellipsoid, major axis roughly east to west and minor axis roughly north to south. The gyres appear as inclusive blue to blue-green regions (CHL > 0.15 mg m^{-3}), ill-defined because of eddy-shedding by the boundary currents. The NAG combines three biogeochemical provinces (as defined by Longhurst et al. 1998), the NATL, NAST (E) and (W); the SAG consists of the SATL alone. These zones are consistent with the oligotrophic biomes identified by Hardman-Mountford et al. (2008).

3.1.1 Physical properties

The NAG is bounded on the pole-ward edge by the strong, easterly-flowing Gulf Stream (GS) and North Atlantic Current (NAC), on the eastern edge by the moderate, southerly Canary Current (CC), on the equatorial edge by the strong and low-salinity North Equatorial Current (NEC) and to the western edge by the weak Antilles Current (AntC). In the TER, between the NEC and the equator, is the west-to-east flowing Equatorial Counter-Current (ECC), an important retro flow to the NEC. It has no influence on the gyre equatorial edge. The SAG is bounded on the equatorial edge by the moderate, westerly, low-salinity South Equatorial Current (SEC), to the western edge by the weak Brazil current (BC), at the pole-ward edge by the strong easterly South Atlantic Current (SAC) and to the eastern edge by the moderate Benguela Current (BenC). Monthly composites of surface geostrophic currents, derived from altimetry are shown in Fig. 4, for January, July, March, September, May and November. Away from the periphery, the images show that the core of the gyres are largely static, with geostrophic current speeds mostly <0.025 m s^{-1}, though there are internal features such as the Azores current in the NAG (at ~33°N) that have speeds of ~0.1 m s^{-1}. The GS and NAC at the pole-ward edge of the NAG have geostrophic current speeds of 0.5 to >0.7 m s^{-1}, which have quasi-consistent locations for all months, but vary in strength seasonally. The same is true of the SAC at the pole-ward edge of the SAG. On its southern edge, the SAC merges with the strong easterly Antarctic Circumpolar Current (ACC).

Figure 5 shows monthly composites of Sea Surface Salinity (SSS) derived from SMOS data (2010-2012), for January, July, March, September, May and October. Both the NEC and SEC are low salinity currents. The NEC has lowest salinity in mid-winter (January) and highest in September (July to October, SSS drops to < 35 PSU), consistent with the maximum intensity of rainfall and location of the intertropical convergence zone (ITCZ) which is predominantly north of the equator. The SEC is much lowest salinity by comparison (rarely < 36 PSU). These observations are consistent with comparisons of AMT *in situ* measurements of SSS and SST on southbound (September to November) and northbound cruises (April to May).

Figure 6 shows the SST climatology (OISST) of the NAG and SAG for the months of March and September (the warmest and coldest months in each gyre), and for the mid-winter and mid-summer months of January (minimum SI in the NAG, and maximum SI in the SAG) and July (maximum SI in the NAG, and minimum SI in the SAG), with the boundary currents overlain. January and July are also key months for CHL (highest in the winter and lowest in the summer, Fig. 7). SST increases in summer and the gyre area (GA) expands, driven by the heat budget (McClain et al. 2004). SST rises by 4°C to 5°C from the pole-ward edge to equatorial edge, in both the NAG and SAG. SST and GA are maximum close to the autumnal equinox (September in the NAG and March in the SAG), lagging the solar maximum by ~2 to 3 months, with minimum SST and GA close to the vernal equinox.

North of 40°N (NAG poleward edge) the isotherms show an east to west alignment for January and March, consistent with deeply-mixed water in winter which stratifies in spring. South of the SAG poleward edge, the isotherms are predominantly east to west and tightly bunched for all seasons, indicative of the strength of the SAC all year long and its impact on the physical oceanography of the region.

3.1.2 Biological properties

Viewed from space (Fig. 3), the STGs (both NAG and SAG) are quasi-ellipsoid but their size and shape changes with season and with inter-annual variability. Figure 7 shows the monthly climatology of CHL (OC-CCI data) for: a) January; b) March; c) May; d) July; e) September; and f) October, with the oligotrophic gyres (low CHL waters) highlighted in blue. Minimum and maximum SST and CHL occur in the months of January, March, July and September, opposite for each gyre (NAG and SAG), while May and October are the months (with September) most frequently sampled by AMT. These monthly climatologies conceal year-to-year variability.

The pole-ward edges of both gyres (Fig. 7) are tightly constrained by the strong boundary currents, as discussed in the previous section. At each boundary, RS CHL changes sharply (<0.15 mg m^{-3} in gyre and >0.15 out of gyre), in support of *in situ* measurements of fluorescence and HPLC from AMT cruises (see Fig. 8). The Tropical Equatorial Region (TER, ~15°N to ~8°S) between the NAG and SAG is generally oligotrophic (CHL generally ~0.15 to 0.2 mg m^{-3}), but shows elevated CHL (Longhurst, 1993, Aiken et al. 2000) consistent with seasonal (and inter-annual) changes in equatorial currents (NEC and SEC, see previous section), and fluctuations in the Mauritanian upwelling (Pradhan et al. 2006), the Amazon and Orinoco outflow (Signorini et al. 1999) and the Congo River (Hardman-Mountford et al. 2003; Hopkins et al. 2013). The boundary currents to the east (CanC in the NAG and BenC in the SAG) constrain the gyres tightly. Western currents (AntC in the NAG and BraC in the SAG) are weaker and offer less constraint, such that oligotrophy extends to the western edge of the Caribbean in the NAG and close to the coast of Brazil in the SAG. In both these regions, the water depth is >1000m so it is possible these areas are permanently thermally stratified. The sharp gradients of CHL at the polar edges in both the NAG and SAG, dropping from >0.2 mg m^{-3} (out) to <0.15 mg m^{-3} (in), constrained by the strong boundary currents (GS in the NAG and SAC in the SAG), indicate that the gyre edges are within this CHL range.

Given the focus on biogeochemistry and carbon cycling, it is appropriate to define the areal extent of the STG by their inherent biological property, oligotrophy (low surface CHL), as a result of low macro-nutrient concentrations. AMT surface and station *in situ* data (to 300m) have been analysed for most AMT cruises, along with contemporary RS composite data of SST and CHL for all cruises, to locate the gyre boundaries. Additionally, we have analysed monthly climatology data (RS) of SST and CHL along a meridional section mid-gyre (40°W in NAG, 25°W in SAG) which show sharp gradients of change at the locations of the gyre edge. Collectively these data are used to define the gyre periphery in the next section.

3.1.3 Definition of Gyre periphery

AMT surface and sub-surface data of temperature, salinity, Chla, and NO_3 (among other variables) are useful for defining the edges of the gyres. The poleward edge of the NAG and SAG shows a sharp rise in SST, salinity and a reduction in CHL (Figs. 8, 9 and 10), with this edge shifting with season (Fig. 9 AMT-17 BFAS and Fig. 10 AMT-14 AFBS). Surface nutrients, principally nitrate, fall sharply to <1 μM at these boundaries, below the limit for photometric analysers (Figs. 9 and 10). The step change of surface CHL generally occurs at around 0.15 mg m^{-3}, consistent with Aiken et al. (2009, see their Figs. 2 and 5), and seen in both *in situ* AMT and RS data (Figs. 7 and 8). The equatorial edges of the NAG and SAG are less distinct when compared with the pole-ward edges. In the TER the surface CHL is typically 0.15 to 0.25 mg m^{-3} (Figs. 7, 8, 9 and 10). The equatorial edges of the two gyres are characterised by sharp gradients in salinity (Figs. 8, 9 and 10, see also Fig. 5).

Vertical sections of temperature, salinity, Chla, and NO_3 (Figs. 9 and 10) show abrupt changes of all the main variables with depth as a result of the changes in water masses at both polar and equatorial edges of the NAG and SAG. Figure 9 and 10 show the 0.1 to 0.15 mg m^{-3} Chla band (azure-blue) outcrops at the surface, co-located with sharp changes in temperature, salinity, and nitrate through the water column. The azure-blue band also defines the depth of the oligotrophic layer; from ~40m at the pole-ward edges to ~80m to ~100m in the centre of the NAG and SAG, depending on season (Figs. 9 and 10). Vertical sections of AMT-17 and AMT-14 data (Figs. 9 and 10, also seen in other cruise data sets), show variations in the depth of the oligotrophic layer (the chloro-cline), and the depth of the DCM. Both these depths have significant empirical relationships with CHL (from RS data, see Brewin et al. (Submitted this issue)). These relationships are exploited in the modelling section below.

At the pole-ward edge of the gyre, the water masses are not permanently thermally stratified but stratified seasonally (spring to fall). Once the surface integrated daily heat flux becomes persistently negative the surface layer cools and induces convection. This convection erodes the seasonal thermocline along with wind driven mixing. When the heat budget goes positive in the spring, thermal stratification is re-established with a warm surface layer that deepens through the spring-summer.

In the TER, two low salinity currents (the NEC and SEC, north and south of the equator) define the edges of the gyres. The TER is salinity-stratified and mostly oligotrophic (Chla < 0.2) but fails to satisfy the STG criteria of thermal stratification. At the equator the EEC and SEC induce a divergent upwelling of nutrient rich water, supporting a CHL peak at the surface (Aiken et al. 2000), varying seasonally and annually (typically > 0.15 to < 1.0 mg m^{-3}), as illustrated in Fig. 8. *In situ* analysis along AMT cruise tracks (Figs. 8, 9 and 10) is consist with analysis of RS data of SST, SSS and CHL along a meridional section mid-gyre (40°W in NAG, 25°W in SAG).

Consolidating all the analyses, we set the criterion that the gyre edge is the 'zone' where the gradient of change is greatest. This 'zone' is arbitrary but with a quantifiable uncertainty. This gradient appears greatest at the boundary of 0.15 mg m^{-3} CHL, though we also use a 0.10 mg m^{-3} CHL boundary for comparison in some analysis.

3.1.4 Seasonal changes in vertical properties of the NAG and SAG

Figure 11a shows RS climatological monthly averages of surface Chla (CHL) and PAR, and average mixed-layer depth derived from de Boyer Montégut et al. 2004, all averaged within each gyre (using a 0.15 mg m^{-3} boundary in CHL). Figure 11b shows seasonal cycles in estimates of the ratio of Chla at the DCM to that at the surface together with climatological monthly averages of PAR, and Figure 11c shows seasonal cycles in integrated Chla (vertically integrated within 1.5 times the euphotic depth) and depth of DCM. The ratios of Chla at the DCM to that at the surface, integrated Chla and depth of DCM in Fig. 11 were estimated by forcing the empirical model of Brewin et al. (Submitted, this issue) with climatological monthly averages of CHL within each gyre (Fig. 11a). Over the seasonal cycle, the ratio of Chla at the DCM to that at the surface varies from about 3 to 5 (Fig. 11b, note that it can be < 3 close to the gyre edge and > 5 towards the centre of the gyre), and the average depth of the DCM (Fig. 11c) is shown to vary between 80 to 100m (< 80m at the gyre periphery and > 100m toward the centre of the gyre). Seasonal variations in the ratio of Chla at the DCM to that at the surface, and the depth of the DCM, are positively correlated with PAR and inversely correlated with CHL and mixed-layer depth. The empirical model predicts a ~5% change in integrated Chla in the SAG and NAG (Fig. 11c), in contrast to a ~25% change in surface Chla (CHL, see Fig. 11a).

Figure 12 shows simulations of SST (Fig. 12a), depth of the DCM (Fig. 12b), surface Chla (averages in the top 40m, Fig. 12c) and DCM Chla (Fig. 12d) from the coupled ERSEM-GOTM model simulations at the centre of the SAG over the period 1997 to 2004. The ERSEM-GOTM simulations (Fig. 12) are generally consistent with the empirical model results in Fig. 11, and show consistent seasonal cycles in SST when compared with RS data (see Fig. 14). The depth of the DCM is deeper in the summer months (Fig. 12b) and shallower in the winter, consistent with the empirical model (Fig. 11), and varies between about 85m in the winter to about 115m in the summer. The model produces a seasonal cycle in CHL (Fig. 12c) that is in agreement with RS estimates for the SAG (Fig. 11a), reproducing the characteristic seasonal cycles in CHL in the SAG (Fig. 12c), with surface concentrations higher in the winter (July) and lower in the summer (January). However, the ERSEM-GOTM simulations predict lower surface Chla (Fig. 12c) than RS (Fig. 11a), likely due to the fact the ERSEM-GOTM was implemented at the centre of the gyre where Hardman-Mountford et al. (2013) observed a small bias (~0.02 mg m^{-3}) between modelled surface Chla and RS. Averaged integrated Chla concentrations from ERSEM-GOTM simulations agree with the empirical model (Fig. 11c) averaging ~20 mg m^{-2} over the year, and are relatively stable (standard deviation 0.8 mg m^{-2}). Chla at the DCM is maximum during the summer (December) and minimum in the winter (May, see Fig. 12d), and is inversely correlated with surface chlorophyll (Fig. 12c).

Simulations from the two contrasting modelling approaches (Fig. 11 and 12) indicate enhanced stratification (shallow mixed-layer), lower surface attenuation (lower surface CHL) and increased solar insolation (increased PAR) in summer months (November to February). In this period, light penetrates deeper into the water column, anallowing the phytoplankton at the DCM to produce more Chla relative to that at the surface, and photosynthesize at deeper depths where nutrient concentrations are higher. Furthermore, the modelling results suggest that in the STGs, seasonal changes in physical forcing (e.g. PAR and mixed-layer) principally act to re-distributed Chla in the water column (Fig. 11b, 12c and 12d), with only a relatively small influence on integrated Chla, despite large relative changes in surface Chla (Hardman-Mountford et al. 2013). These two modelling approaches emphasise the importance of considering changes in Chla throughout the water column, for a more holistic understanding the impact of environmental change on marine ecosystems. Future work incorporating bio-Argo data together with RS and modelling (Mignot et al. 2014) should shed further light on seasonal changes in the vertical properties of the NAG and SAG.

3.2 Seasonal and inter-annual changes in gyre area, SST, CHL and PAR

3.2.1 Seasonal changes between 1998 and 2012

Figures 13 and 14 show the seasonal cycles of SST, gyre area (GA), CHL and PAR (PAR data incomplete after 2008) in NAG and SAG over the period 1998 to 2012, determined from RS using gyre boundary limits of 0.10 and 0.15 mg m^{-3}. Mean values of SST and PAR are comparable for both boundaries (e.g. SST minimum 23.1°C, mean 25.4°C, and max 27.5°C). This implies mean values of SST and PAR are representative of those close to the gyre centres. SST, driven by the heat budget, lags PAR by 2-3 months. SST is warmest in September (NAG) and coldest in March (NAG), three months after the winter solstice (vice versa in the SAG, Fig. 13 and 14). The GA changes considerably for each boundary (boundary limit of 0.10 mg m^{-3} and 0.15 mg m^{-3}), with a minimum of 4.5 x 10 km^2 to 9.2 x 10 km^2, mean 10.7 x 10 km^2 to 15.0 x 10 km^2, and maximum 15.8 x 10 km^2 to 19.4 x 10 km^2. The gyres expand only slightly at the poleward edge and equatorial edge in summer, but there is a large expansion on the east-west axis. The GA is directly correlated with SST and PAR (Fig. 13 and 14). Typically, SST lags GA by a month as a result of the decline of CHL from mid-winter high, before the SST minimum. CHL is max in January (NAG) and July (SAG), inversely correlated with PAR, and out of phase with SST. The sharp peak of CHL in mid-winter results from the dependence on the flux of nutrients out of the nutracline zone, controlled by declining productivity in the DCM.

3.2.1 Inter-annual variations and trends

Figures 15 and 16 show monthly anomalies of GA, CHL, SST and PAR, for the NAG and SAG, with the Multivariate ENSO Index (MEI) for the same period. In the NAG there is an upward trend for CHL and SST (both significant at the 99% percent level), slight downward trend for PAR (significant at the 83% percent level) and upward trend for GA (significant at the 81% percent level). Increasing CHL with decreasing PAR could be a manifestation of the 'Light Effect' (Taylor, Harris and Aiken 1986), or possibly changes in photoacclimation (Behrenfeld et al. 2015). It is possible that increased aerosols (water vapour, dust input and clouds) from anthropogenic and natural sources in the northern hemisphere over this period (Tan et al. 2011), may have impacted PAR and CHL.

In the SAG, CHL shows an upward trend (significant at the 99% percent level) with slight upward trend for PAR (significant at the 87% percent level), and no significant trend in GA and SST. For both NAG and SAG, the anomalies for CHL and SST show traits that reflect the El Niño and La Niña (MEI) episodes. Considering the relatively short length of satellite time-series data used in this study (1998-2012), one need to be cautious when relating changes to longer term global warming trends, considering one requires >40 year of CHL data to distinguish a global warming trend from natural variability, depending on region (Henson et al. 2010). Increases in CHL in both the NAG and SAG over the 1998-2012 period are consistent with other trend analysis methods (Vantrepotte and Mélin, 2011) conducted using OC-CCI data over the same time period and in the regions of the NAG and SAG (Sathyendranath & Krasmann et al. 2014, see their Fig 5-9).

4. Summary

The prime objectives of AMT were to exploit *in situ* measurements, RS observations of key physical and biogeochemical variables, combined with modelling, to address issues of the impact of global warming and climate change on the ecosystems of the Atlantic Ocean 50°N to 50°S. A supplementary goal was to acquire high quality bio-optical and biological data to assist the calibration and validation of RS ocean-colour products in a wide range of ocean ecosystems. To this goal the AMT activities have played a substantive role and enhanced RS data validation by exploiting precision in-water optical systems and new techniques for validation (e.g. Dall'Olmo et al. 2012; Brewin et al. Submitted), and will likely continue this role in the future as new ocean-colour missions are launched (e.g. ESA Sentinel-3).

In this study, we provide a synthesis of the key physical and biogeochemical properties on the North and South Atlantic sub-tropical gyres (NAG, SAG), providing insight for other studies of process rates and air-sea exchange of biogenic gases. Surface and sub-surface data of physical variables (temperature and salinity) and biogeochemical variables (Chla, Nitrate) to >300m, coupled with RS data of SST, SSS, CHL, PAR and surface geostrophic currents (from altimetry), and two modelling approaches (Brewin et al. Submitted this issue; Hardman-Mountford et al. 2013), are used to describe the basic physical and biological characteristics of the NAG and SAG.

At the surface of the gyres, the limited seasonal coverage by AMT cruises are augmented by RS data for weekly, monthly and annual composites and decadal time series. The AMT *in situ* data have helped define gyre boundaries. These data have been complemented by RS for observations of SST and CHL that provide data for the whole gyre area. Surface geostrophic currents show the very low velocity flow (<0.03 m s^{-1}) for the internal gyre entity and highlight the high velocity flow at the gyre edges (NAC, NEC, SEC, SAC, velocity >0.7 m/s) that constrain the gyre zones. SSS measurements show the location and velocity of the equatorial boundary currents (NEC, SEC) and the low salinity zone of the

ITCZ that feed these systems. The defining inherent characteristics of the STGs are their permanent thermal stratification and oligotrophy (low macro-nutrient concentration, and low surface Chla biomass). The analyses of AMT data provide strong evidence that the gyre boundaries occur at a value close to 0.15 mg m^{-3} Chla with some uncertainty, coinciding with the sharpest gradient of the main variables. AMT *in situ* data show abrupt changes of all the main variables with depth as a result of changes in water masses at both polar and equatorial edges of the NAG and SAG (Figs. 9 and 10). RS surface data of SST, SSS and distinctively CHL, also provide robust location of the gyre edges, agreeing with *in situ* data estimates. Meridional sections of SST, CHL and geostrophic currents along pseudo-transects through the centres of the gyres at 40°W (NAG) and 25°W (SAG) further support our definition of gyre boundaries (available as supplementary data on request). RS data highlight significant increases in CHL within the gyre over the duration of the AMT transect.

Two modelling approaches are described that provide means for extrapolating RS observations to greater depths using AMT observations and empirical relationships. From RS CHL we can determine Chla in the DCM and throughout the water column and other properties (e.g. the chloro-cline, which aligns with the nutrient depleted surface layer). The coupled ecosystem/physical model can provide simulated seasonal cycles at all locations and aid deficiencies in AMT sampling from temporal coverage and spatial aliasing of similar cruise tracks. Modelling results illustrate that seasonal changes in physical forcing (e.g. PAR and mixed-layer) act to re-distributed Chla in the water column over the season.

The synthesis of AMT data, RS observations and modelling provides a comprehensive insight into the coupled physical and bio-optical processes controlling the seasonal dynamics of productivity and biomass in the STGs. In essence the STGs are two-layer systems: the surface layer (quasi-mixed) is nutrient depleted (N-limited) but in light luxury; the DCM is relatively nutrient replete, but light limited. Both change seasonally and counter intuitively the highest surface Chla in both gyres is in mid-winter when SI is least. This is a manifestation of the Light Effect (Taylor, et al, 1986), where SI regulates the vertical distribution of productivity, nutrient supply and Chla in a stratified ecosystem. Productivity and Chla in the DCM are maximum in mid-summer but decline thereafter as SI diminishes, releasing nutrients to the surface layer and enhancing surface production and Chla. The effect is amplified by positive feedback; increased Chla in the surface layer absorbs light, diminishing DCM production and nutrient consumption. After the winter solstice, SI increases, production in the DCM increases, reducing the flux of nutrients to the surface layer, surface productivity and Chl.

Despite similarities in the general functioning of the NAG and SAG (e.g. changes in chlorophyll in response to seasonal forcing), the two gyres are recognised as having distinct differences in some biogeochemical characteristics not investigated here. For example, the NAG has significant dust input which is thought to encourage nitrogen-fixation and the draw-down of phosphate to lower levels than seen in the SAG (Reynolds et al. 2007, Mather et al. 2008). Furthermore, despite both gyres showing significant increases in CHL during the study period, differences in trends for physical properties were not always consistent (Figs. 15 and 16). For instance, the NAG shows an upward trend for SST (> 99% level), a slight upward trend for GA ($p = 0.19$), and a slight downward trend in PAR ($p = 0.17$, Fig. 15). This is likely indicative of global warming leading to gyre expansion, and increased atmospheric attenuation (e.g. from increases in either: evaporation; water vapour (a greenhouse gas); cloudiness due to global warming; anthropogenic aerosols (fossil fuel burning); or natural aerosols (e.g. Saharan dust)). Alternatively, in the SAG no significant trends were seen in SST and GA (Fig. 16), though ocean heat content is known to increase in the SAG (Levitus et al. 2012). These results suggest the physical processes responsible for an increase in CHL may differ between gyres, which may further inform the debate on the autotrophic/heterotrophic status of the surface layer the gyres. Such research might benefit from reference to monthly, seasonal and decadal time series data sets exploited in this study. Synergistically combining AMT data, RS observations and modelling allow for 3D visualizations of gyre basins, that in the future, may be complimented by the ever expanding Argo and bio-Argo network. Nonetheless, caution needs to be taken when extrapolating *in situ* empirical relationships derived at specific times of the year on an AMT cruise (Spring / Autumn) to the whole year. For a truly robust basis, *in situ* data are also required for the keystone months of January and July, and a small number of dedicated cruises targeting the NAG and SAG during these months could help solve this issue.

ACKNOWLEDGEMENTS

Data was used from the Atlantic Meridional Transect (AMT) Consortium (NER/0/5/2001/00680), provided by the British Oceanographic Data Centre (BODC) and supported by the Natural Environment Research Council National Capability funding to Plymouth Marine Laboratory and the National Oceanography Centre, Southampton. We sincerely thank officers and crew of the RRS James Clark Ross, RRS James Cook and RRS Discovery, for their help during the AMT cruises and all those involved in data collection and analysis. We also thank NERC, BAS, PML, CCMS, SOC, NOC, NASA and MOD

(Hydrographic Office) for AMT support. We thank the founder partners of AMT, Holligan, Watson, Robins, Harris, Bale, N. Rees, Hooker and interim and current leaders and PSOs, Woodward, Robinson, A. Rees, Smyth, Zubkov and Tarran.

The authors would like to thank all space agencies for remote-sensing data, without which this work would not have been feasible. We thank NEODAAS for support. We thank the ESA for data from the OC-CCI, and SMOS, NASA for the processing and distribution of the SeaWiFS and AVHRR data. The altimeter products were produced by Ssalto/Duacs and distributed by AVISO, with support from CNES (http://www.aviso.oceanobs.com/duacs/). We also thank NOAA for OISST products. This work is supported by the UK National Centre for Earth Observation and is a contribution to the Ocean Colour Climate Change Initiative of ESA. This is also contribution number xxx of the AMT programme.

REFERENCES

Aiken, J., Rees, N., Hooker, S., Holligan, P., Bale, A., Robins, D., Moore, G., Harris, R., Pilgrim, D. (2000). The Atlantic Meridional Transect: overview and synthesis of data. *Progress in Oceanography* **45** (3-4), 257-312.

Aiken, J., Pradhan, Y., Barlow, R., Lavender, S., Poulton, A., Holligan, P., Hardman-Mountford, N. (2009). Phytoplankton pigments and functional types in the Atlantic Ocean: A decadal assessment, 1995-2005. *Deep-Sea Research Part II-Topical Studies in Oceanography* **56** (15), 899-917.

Behrenfeld, M.J., O'Malley, R.T., Boss, E.S., Westberry, T.K., Graff, J.R., Halsey, K.H., Milligan, A.J., Siegel, D.A., & Brown, M.B. (2015) Revaluating ocean warming impacts on global phytoplankton. *Nature Climate Change*. doi: 10.1038/NCLIMATE2838

Bindoff, N.L., Willebrand, J., Artale, V., Cazenave, A., Gregory, J.M., Gulev, S., Hanawa, K., Le Quéré, C., Levitus, S., Nojiri, Y., Shum, C.K., Talley, L.D. and Unnikrishnan, A.S. (2007) *Observations: Oceanic Climate Change and Sea Level.* In: Climate Change 2007: The Physical Science Basis. Cambridge University Press, pp. 385-432. ISBN 0521705967

Blackford JC, Allen JI, Gilbert FJ. 2004 Ecosystem dynamics at six contrasting sites: a generic modelling study. *J. Mar. Syst.* **52**, 191–215, doi:10.1016/j.jmarsys.2004.02.004

Brewin, R.J.W., Dall'Olmo, G., Pardo, S. van Dongen-Vogel, V., Boss, E. S. (2016) Underway spectrophotometry along the Atlantic Meridional Transect reveals high performance in satellite chlorophyll retrievals. *Remote Sensing of Environment*, **183**. 82-97. 10.1016/j.rse.2016.05.005

Brewin, R. J. W., Mélin, F., Sathyendranath, S., Steinmetz, F., Chuprin, A., Grant, M., (2014). On the temporal consistency of chlorophyll products derived from three ocean-colour sensors. *ISPRS Journal of Photogrammetry and Remote Sensing* **97**, 171–184.

Brewin, R. J. W., Sathyendranath, S., Hirata, T., Lavender, S., Barciela, R. M., & Hardman-Mountford, N. J. (2010). A three-component model of phytoplankton size class for the Atlantic Ocean. *Ecological Modelling*, **221**, 1472−1483.

Brewin, R. J. W., Sathyendranath, S., Müller, D., Brockmann, C., Deschamps, P-Y., Devred, E., Doerffer, R., Fomferra, N., Franz, B., Grant, M., Groom, S., Horseman, A., Hu, C., Krasemann, H., Lee, Z., Maritorena, S., Mélin, F., Peters, M., Platt, T., Regner, R., Smyth, T., Steinmetz, F., Swinton, J., Werdell, J. & White, G.N. (2015) The Ocean Colour Climate Change Initiative: III. A round-robin comparison on in-water bio-optical algorithms. *Remote Sensing of Environment*, **162**, 271-294. doi:10.1016/j.rse.2013.09.016

Brewin, R.J.W., Tilstone, G., Cain, T., Miller, P., Lange, P., Misra, A. Airs, R. & Jackson, T. (Submitted to this issue) Modelling size-fractionated primary production in the Atlantic Ocean from remote-sensing: a filtration-based parameterisation. *Progress in Oceanography*

Burchard, H., Bolding, K., Villareal, M. (1999) GOTM: a general ocean turbulence model. Theory, applications and test cases. Technical Report EUR 18745 EN. European Commission, Brussels, Belgium.

Dall'Olmo, G., Boss, E., Behrenfeld, M. & Westberry, T. K. (2012). Particulate optical scattering coefficients along an Atlantic Meridional Transect. *Optics Express* **20**, 21532–21551.

de Boyer Montégut, C., Madec, G., Fisher, A.S., Lazar, A., Iudicone, D. (2004). Mixed layer depth over the global ocean: an examination of profile data and a profile based climatology. *Journal of Geophysical Research* **109**, C12003.

Font, J., Camps, A., Borges, A., Martín-Neira, M., Boutin, J., Reul, N., Kerr, Y. H. Hahne, A. & Mecklenburg, S. (2010). SMOS: The challenging sea surface salinity measurement from space. *Proceedings of the IEEE*, 98(5), 649-665.

Goldenberg, S.B., Landsea, C.W., Mestas-Nuñez, A.M. & Gray, W. M. (2001) The Recent Increase in Atlantic Hurricane Activity: Causes and Implications. *Science*, **293**, 474-479, doi:10.1126/science.1060040

Hardman-Mountford, N.J., Agenbag, J.J., Hagen, E., Nykjaer, L., Richardson, A.J., Shillington, F. & Villacastin, C. (2003). Ocean climate of the South East Atlantic observed from satellite data and wind models. *Progress in Oceanography* **59** (2-3): 181-222.

Hardman-Mountford, N.J., Hirata, T., Richardson, K.A. & Aiken, J. (2008). An objective methodology for the classification of ecological pattern into biomes and provinces for the pelagic ocean. *Remote Sensing of Environment* **112**, 3341-3352. doi:10.1016/j.rse.2008.02.016

Hardman-Mountford, N.J., Polimene, L., Hirata, T., Brewin, R.J.W. & Aiken, J. (2013) Impacts of light shading and nutrient enrichment geo-engineering approaches on the productivity of a stratified, oligotrophic ocean ecosystem. *J R Soc Interface* **10**: 20130701. doi:10. 1098/rsif.2013.0701

Henson, S.A., Sarmiento, J.L., Dunne, J.P., Bopp, L., Lima, I., Doney, A.C., John, J., Beaulieu, C. (2010). Detection of anthropogenic climate change in satellite records of ocean chlorophyll and productivity. *Biogeosciences* **7**, 621–640, doi:10.5194/bg-7-621-2010.

Hirata, T., Aiken, J., Hardman-Mountford, N. J., Smyth, T. J., & Barlow, R. G. (2008). An absorption model to derive phytoplankton size classes from satellite ocean colour. *Remote Sensing of Environment*, **112**(6), 3153−3159.

Holt, J., Allen, J. I., Anderson, T. R., Brewin, R. J. W., Butenschön, M., Harle, J., Huse, G., Lindemann, C., Memery, L., Salihoglu, B., Senina, I., & Yool, A. (2014) Challenges in integrative approaches to modelling the marine ecosystems of the North Atlantic: Physics to fish and coasts to ocean, *Progress in Oceanography*, **129**, 285-313. doi: 10.1016/j.pocean.2014.04.024

Hopkins, J., Lucas, M., Dufau, C., Sutton, M., Stum, J., Lauret, O., & Channelliere, C. (2013). Detection and variability of the Congo River plume from satellite derived sea surface temperature, salinity, ocean colour and sea level. *Remote Sensing of Environment*, **139**, 365-385, doi:10.1016/j.rse.2013.08.015

Kitidis, V., Brown, I., Hardman-Mountford, N. J., Lefèvre, N. (Submitted this issue) Surface ocean carbon dioxide during the Atlantic Meridional Transect (1995-2013); evidence of ocean acidification. *Progress in Oceanography*

Le Quéré, C., Moriarty, R., Andrew, R. M., Peters, G. P., Ciais, P., Friedlingstein, P., Arneth, A. (2014). Global carbon budget 2014. *Earth Syst. Sci. Data Discuss*., **7**(2), 521–610. doi:10.5194/essdd-7-521-2014.

Levitus, S., Antonov, J., Boyer, T. P., and Stephens, C. (2000) Warming of the world ocean, *Science*, **287**, 2225-2229, doi:10.1126/science.287.5461.2225

Levitus, S., Antonov, J. L., Wang, J., Delworth, T. L., Dixon, K. W. and Broccoli, A. J. (2001), Anthropogenic warming of Earth's climate system, *Science*, **292**, 267-270, doi:10.1126/science.1058154

Levitus, S., Antonov, J. L., and Boyer T.P. (2005), Warming of the world ocean, 1955-2003, *Geophys. Res. Lett.*, **32**, L02604, doi:10.1029/2004GL021592

Levitus, S., Antonov, J.I., Boyer, T.P., Baranova, O.K., Garcia, H.E., Locarnini, R.A., Mishonov, A.V., Reagan, J.R., Seidov, D., Yarosh, E.S. and Zweng, M.M. (2012). World ocean heat content and thermosteric sea level change (0-2000m), 1955–2010. *Geophysical Research Letters*, 39(10).

Longhurst, A. (1993), Seasonal cooling and blooming in the tropical oceans, *Deep Sea Res., Part I*, **40**, 2145–2165.

Longhurst, A., (1998). *Ecological geography of the sea*. San Diego: Academic Press.

Mather, R.L., Reynolds, S.E., Wolff, G.A., Williams, R.G., Torres-Valdes, S., Woodward, E.M.S., Landolfi, A., Pan, X., Sanders, R. & Achterberg, E.P. (2008). Phosphorus cycling in the North and South Atlantic Ocean subtropical gyres. *Nature Geoscience*, **1**(7), 439-443.

Meehl, G. A., Arblaster, J. M., Fasullo, J. T., Hu, A., & Trenberth, K. E. (2011). Model-based evidence of deep-ocean heat uptake during surface-temperature hiatus periods. *Nature Climate Change*, **1**(7), 360-364.

McClain, C.R. (2009) A Decade of Satellite Ocean Color Observations. *Annual Review of Marine Science*, 1, 19-42, doi: 10.1146/annurev.marine.010908.163650.

McClain, C. R., Signorini, S. R. and Christian, J. R. (2004) Subtropical gyre variability observed by ocean-color satellites, *Deep Sea Research Part II: Topical Studies in Oceanography*, **51**, 281-301, doi:10.1016/j.dsr2.2003.08.002

Merchant, C. J., Embury, O., Rayner, N. A. , Berry, D. I., Corlett, G., Lean, K., Veal, K. L., Kent, E. C., Llewellyn-Jones, D., Remedios, J. J. and Saunders, R. (2012) A twenty-year independent record of sea surface temperature for climate from Along-track Scanning Radiometers. *Journal of Geophysical Research*, **117**. C12013. ISSN 0148-0227 doi: 10.1029/2012JC00840

Mignot, A., Claustre, H., Uitz, J., Poteau, A., D'Ortenzio, F. and X. Xing (2014) Understanding the seasonal dynamics of phytoplankton biomass and DCM in oligotrophic environments: a Bio-Argo float investigation. *Global Biogeochemical Cycles*, **28**, doi: 10.1002/2013GB004781

Morel, A. & Berthon, J.F. (1989). Surface pigments, algal biomass profiles, and potential production of the euphotic layer: relationships reinvestigated in view of remote sensing applications. *Limnology and Oceanography* **34** (8), 1545–1562.

Müller, D., Krasemann, H., Brewin, R. J. W., Brockmann, C., Deschamps, P-Y., Doerffer, R., Fomferra, N., Franz, B.A., Grant, G., Groom, S., Mélin, F., Platt, T., Regner, P., Sathyendranath, S., Steinmetz, F. & Swinton, J., (2015a) The Ocean Colour Climate Change Initiative: I An Assessment of Atmospheric Correction Processors based on in-situ measurements. *Remote Sensing of Environment* **162**, 242-256. doi:10.1016/j.rse.2013.11.026

Müller, D., Krasemann, H., Brewin, R. J. W., Brockmann, C., Deschamps, P-Y., Doerffer, R., Fomferra, N., Franz, B.A., Grant, G., Groom, S., Mélin, F., Platt, T., Regner, P., Sathyendranath, S., Steinmetz, F. & Swinton, J., (2015b) The Ocean Colour Climate Change Initiative: II Spatial and Seasonal Homogeneity of Atmospheric Correction Algorithms. *Remote Sensing of Environment* **162**, 257-270. doi:10.1016/j.rse.2015.01.033

Platt, T., Sathyendranath, S. (1988). Oceanic primary production: Estimation by remote sensing at local and regional scales. *Science* **241**, 1613–1620.

Polimene, L., Archer, S.D., Butenschon, M. & Allen, J.I. (2012) A mechanistic explanation of the Sargasso Sea DMS 'summer paradox'. *Biogeochemistry*, **110**, 243–255. doi:10.1007/s10533-011-9674-z.

Polovina, J.J., Howell, E.A. and Abecassis M. (2008) Ocean's least productive waters are expanding, *Geophys. Res. Lett.*, **35**, L03618, doi:10.1029/2007GL031745.

Pörtner, H.-O., Karl, D., Boyd, P.W., Cheung, W., Lluch-Cota, S.E., Nojiri, Y., Schmidt, D.N. and Zavialov P. (2014): Ocean systems. In: *Climate Change 2014: Impacts, Adaptation, and Vulnerability. Part A: Global and Sectoral Aspects*. Contribution of Working Group II to the Fifth Assessment Report of the Intergovernmental Panel on Climate Change [Field, C.B., Barros, V.R., Dokken, D.J., Mach, K.J., Mastrandrea, M.D., Bilir, T.E., Chatterjee, M., Ebi, K.L., Estrada, Y.O., Genova, R.C., Girma, B., Kissel, E.S., Levy, A.N., MacCracken, S., Mastrandrea, P.R. and White L.L. (eds.)]. Cambridge University Press, Cambridge, United Kingdom and New York, NY, USA, pp. 411-484.

Pradhan, Y.,Lavender, S.J., Hardman-Mountford, N.J. and Aiken, J. (2006) Seasonal and inter-annual variability of chlorophyll-a concentration in the Mauritanian upwelling: Observation of an anomalous event during 1998–1999. *Deep-Sea Research II* **53**, 1548–1559, doi:10.1016/j.dsr2.2006.05.016.

Reynolds, S.E., Mather, R.L., Wolff, G.A., Williams, R.G., Landolfi, A., Sanders, R. and Woodward, E.M.S. (2007) How widespread and important is N2 fixation in the North Atlantic Ocean? *Global Biogeochemical Cycles*, **21**(4).

Robinson, C., Poulton, A. J., Holligan, P. M., Baker, A. R., Forster, G., Gist, N., Jickells, T. D., Malin, G., Upstill-Goddardd, R., Williams, R. G., Woodward, E. M. S., Zubkov, M. V., 2006. The Atlantic Meridional Transect (AMT) Programme: A contextual view 1995-2005. *Deep Sea Research II* **53**, 1485–1515.

Sathyendranath, S., & Krasemann, H. (2014). Climate assessment report: Ocean Colour Climate Change Initiative (OC-CCI) — Phase one. http://www.esa-oceancolour-cci.org/?q=documents

Signorini, S. R, Franz, B. A. & McClain, C. R. (2015) Chlorophyll Variability in the Oligotrophic Gyres: Mechanisms, Seasonality and Trends. *Frontiers in Marine Science*, **2**, 1. doi: 10.3389/fmars.2015.00001

Signorini, S.R., Murtugudde, R.G., McClain, C.R., Christian, J.R., Picaut, J. and Busalacchi, A.J. (1999) Biologcal and physical signatures in the tropical and subtropical Atlantic. *Journal of Geophysical Research: Oceans*, **104**, 18,367-18,382, doi: 10.1029/1999JC900134

Slade, W. H., Boss, E., Dall'Olmo, G., Langner, M. R., Loftin, J., Behrenfeld, M. J., Roesler, C. & Westberry, T. K. (2010). Underway and moored methods for improving accuracy in measurement of spectral particulate absorption and attenuation. *Journal of Atmospheric and Oceanic Technology* **933** 27, 1733–1746.

Tan, S-C., Shi, G-Y., Shi, J.H., Gao, H-W., Yao, X. (2011) Correlation of Asian dust with chlorophyll and primary productivity in the coastal seas of China during the period from 1998 to 2008. *Journal of Geophysical Research: Biogeosciences*. **116**, G02029, doi:10.1029/2010JG001456.

Taylor A.H., Harris, J.R.W., Aiken J. (1986) *The interaction of physical and biological processes in a model of the vertical distribution of phytoplankton under stratification*. In Marine interfaces echohydrodynamics (ed. JCJ Nihoul), pp. 313–330. Amsterdam, The Netherlands: Elsevier Science.

Tollefson, J. (2014). Climate change: The case of the missing heat. *Nature*, **505**(7483), 276-278.

Tomczak, M. & Godfrey, J. S. (1994) *Regional oceanography: An introduction*. Pergamon (Oxford), 1994. pp 422

Uitz, J., Claustre, H., Morel, A., Hooker, S.B. (2006). Vertical distribution of phytoplankton communities in open ocean: an assessment based on surface chlorophyll. *Journal of Geophysical Research* **111**, CO8005.

Vantrepotte, V., Mélin, F. (2011). Inter-annual variations in the SeaWiFS global chlorophyll a concentration (1997-2007), *Deep Sea Res. II* **58**, 429–441. Dio:10.1016/j.dsr.2011.02.003.

Wara, M. W., Ravelo, A. C. & DeLaney, M. L. (2005). Permanent El Niño-like conditions during the Pliocene warm period. *Science* **309**, 758–761.

Welschmeyer N.A., 1994. Fluorometric analysis of chlorophyll-a in the presence of chlorophyll-b and phaeopigments. *Limnology and Oceanography*, **39**:1985-1992

Table 1 Glossary of abbreviations and acronyms.

	Agencies, Missions, Ships, Satellites
AMT	Atlantic Meridional Transect; NERC (UK) Oceanographic research programme covering the Atlantic Ocean from 50N to 50S
NERC	Natural Environment Research Council, UK
PRIME	Plankton Reactivity in the Marine Environment (NERC Special Topic research theme)
IPCC	International panel on Climate Change (Intergovernmental)
IGBP	International Geosphere-Biosphere Programme
NASA	National Atmospheric and Space Administration (USA)
NOAA	National Oceanic and Atmospheric Administration (USA)
ESA	European Space Agency (EU)
NASDA	National Space Development Agency (Japan)
ECWMF	European Centre for Medium-Range Weather Forecasts
NEODAAS	NERC Earth Observation Data Acquisition and Analysis Service
RS	Remote Sensing (sensors in space or data from satellite sensors)
AVHRR	Advanced Very High Resolution Radiometer
ATSR	Along Track Scanning Radiometers
AATSR	Advanced Along-Track Scanning Radiometer
CZCS	Coastal Zone Color Scanner
OCTS	Ocean Color and Temperature Sensor on Advanced Earth Observing Sensor (Japan)
SeaWiFS	Sea-Viewing Wide Field-of-View Sensor
MODIS	Moderate Resolution Imaging Spectroradiometer
MERIS	MEdium Resolution Imaging Spectrometer
SMOS	Soil Moisture and Ocean Salinity
OC-CCI	Ocean Colour Climate Change Initiative
OISST	NOAA Optimum Interpolation (OI) SST V2 data
ERSEM	European Regional Seas Ecosystem Model
JCR	RRS James Clark Ross (NERC, BAS Research Vessel)
JC	RRS James Cook (NERC Research Vessel)
Disco	RRS Discovery (NERC Research Vessel)
	Physical and biogeochemical variables (and units)
T	Temperature (°C or K)
Temp	Temperature (°C or K)
C	Conductivity, used to calculate Salinity with Temp
D	Depth as in CTD profiling instrument assemblage (m or db)
Sal	Salinity (PSU)
SST	Sea Surface Temperature (measured on research vessel or from RS) (°C or K)
SSS	Sea Surface Salinity (derived from RS radiometry) (PSU)
OHC	Ocean Heat Content (Joules)
GA	Gyre Area (Km^2)
Chla	Chlorophyll-a photosynthetic pigment in phytoplankton, measured by filtering plankton water sample (surface or selected depths) extracted in solvent (acetone or methanol) and measured in vitro by fluorometer (calibrated with standard sample) or High Performance Liquid Chromatograph (HPLC, calibrated with standard sample) ($mg\ m^{-3}$)

Chlf	Chla measured by flow throw fluorometer, in vitro (on board vessel) or in vivo (profiled or towed instrument) and vicariously calibrated with discrete samples of Chla (mg.m^{-3})
CHL	Surface Chla determined either *in situ* (HPLC or extracted in solvent) or by vicariously calibrated algorithm from RS radiometer in space measuring Ocean Colour in several visible bands (mg.m^{-3})
ACS	Absorption and Attenuation Coefficients sensor
PAR	Photosynthetically Active Radiation, calculated from RS data (or measured) (uE m^{-2} s^{-1})
SI	Solar Insolation (total UV, visible. Near IR and far IR) (W.m^{-2})
DCM	Deep Chlorophyll Maximum (depth of) (m)
SML	Surface Mixed Layer (m)
SL	Surface Layer, above thermocline when layer not totally homogeneously mixed (m)
MLD	Mixed Layer Depth (m)
MADT	Mean absolute dynamic topography (m)

General abbreviations

STG	Sub-Tropical Gyre
NAG	North Atlantic STG
SAG	South Atlantic STG
TER	Tropical Equatorial Region
GS	Gulf Stream
NAC	North Atlantic Current, NW extension of the GS
SAC	South Atlantic Current
NEC	North Equatorial Current
SEC	South Equatorial Current
EUC	Equatorial Under Current
CC	Canaries Current
BC	Brazil Current
BenC	Benguela Current
AntC	Antilles Current
AC	Azores Current
BFAS	South-bound AMT cruises from the UK (September, October and November) sampling the NAG during the boreal fall and transecting the SAG during the austral spring.
AFBS	North bound AMT cruises from either the Falkland Islands or Cape Town (typically April and May), sampling the South Atlantic in the austral fall and the North Atlantic in spring (hereafter denoted AFBS cruises

Figure 1. Global temperatures and atmospheric CO_2 concentrations from 1978 – 2010 at Mona Loa, Hawaii (Northern hemisphere); time spans of Remote Sensing (RS) data sets and AMT cruises. GISS refers to the analysis by NASA's Goddard Institute for Space Studies; HadCRUT3 refers to the third revision of analysis by the UK Met Office Hadley Centre and Climate Research Unit of the University of East Anglia; and NCDC refers to analysis by NOAA's National Climatic Data Centre. The plot was adapted from https://ourchangingclimate.wordpress.com/2010/04/11/recent-changes-in-the-sun-co2-and-global-average-temperature-little-ice-age-onwards/ (accessed 05/05/15)

Figure 2. Annual and seasonal coverage of AMT cruises from AMT-1 through to AMT-25 (1995-2015). Green indicates cruise sector in the northern hemisphere (mostly NAG) and blue indicates cruise sector in the southern hemisphere (mostly SAG).

Figure 3. Atlantic CHL composites from OCTS (AMT-4) and OC-CCI (AMT-5 to AMT22) with AMT cruise tracks overlain. Including: AMT-4 (AFBS, 21/04/97 to 27/05/97); AMT-5 (BFAS, 14/09/97 to 17/10/97); AMT-14 (AFBS, 26/04/04 to 2/06/04); AMT-17 (BFAS, 15/10/05 to 28/11/05); AMT-19 (BFAS, 13/10/09 to 1/12/09); and AMT-22 (BFAS, 10/10/12 to 24/11/12).

Figure 4. Monthly climatology of sea-surface height (SSH) and surface-geostrophic-current derived from AVISO altimetry data for the Atlantic Ocean for: a) January; b) March; c) May; d) July; e) September; and f) November. The magnitude speed (background shading on a log scale) is overlaid with SSH contours at 0.2 m intervals. Grey (blue) contours show regions of positive (negative) SSH, with the zero SSH line shown in black. Current direction is shown in the green, arrow-annotated, streamlines.

Figure 5. The monthly composites of Sea Surface Salinity (SSS) derived from SMOS in the Atlantic Ocean for: a) January; b) March; c) May; d) July; e) September; and f) October.

Figure 6. Monthly climatology of Sea Surface Temperature, derived from OISST data, for January, July, March and September, with a schematic of main current systems overlain, including: 1 = North Atlantic Current (NAC); 2 = Canaries Current

(CC); 3 = North Equatorial Current (NEC); 4 = Antilles Current (AntC); 5 = South Equatorial Current (SEC); 6 = Brazil Current (BC); 7 = South Atlantic Current (SAC); and 8 = Benguela Current (BenC). Breadth of arrows represents strength of flow with purple infill for low salinity currents.

Figure 7. Monthly climatology of CHL (OC-CCI data 14 year composite) in the Atlantic Ocean for: a) January; b) March; c) May; d) July; e) September; and f) October.

Figure 8. Along-track AMT-22 data on: surface temperature (SST, denoted Temp in the figure); Salinity (SSS); surface Chla fluorescence (CHL); and surface Chla (CHL) derived from HPLC from discrete surface water samples taken along-track, and from measurements from an ACS. Measurements are from pumped surface-layer water (nominally 5 m depth) measured continuously by shipboard instruments, illustrating the sharp change of all variables at the gyre edges. Dashed lines show the approximate locations of the gyres edges (North Atlantic Gyre (NAG) and South Atlantic Gyre (SAG)), the South Atlantic Current (SAC), South Equatorial Current (SEC), North Equatorial Current (NEC) and North Atlantic Current (NAC). Black horizontal line on the bottom plot shows the 0.15 mg m^{-3} CHL boundary.

Figure 9. Contoured vertical sections of Nitrate, Chla, Temp, Salinity for AMT-17, with the approximate locations of the gyres edge with the South Atlantic Current (SAC), South Equatorial Current (SEC), North Equatorial Current (NEC) and North Atlantic Current (NAC). Figures were adapted from AMT cruise report 17, available at http://www.amt-uk.org/pdf/AMT17_report.pdf.

Figure 10. Contoured vertical sections of Nitrate, Chla, Temp, Salinity for AMT-14, with the approximate locations of the gyres edge with the South Atlantic Current (SAC), South Equatorial Current (SEC), North Equatorial Current (NEC) and North Atlantic Current (NAC). Figures were adapted from AMT cruise report 14, available at http://www.amt-uk.org/pdf/AMT14_report.pdf.

Figure 11. (a) RS climatological monthly averages of surface Chla (CHL) and PAR, and average mixed-layer depth, all averaged within each gyre (using a 0.15 mg m^{-3}

boundary in CHL). (b) seasonal cycles in estimates of the ratio of Chla at the DCM to that at the surface together with climatological monthly averages of PAR, and (c) seasonal cycles integrated Chla (vertically integrated within 1.5 times the euphotic depth) and depth of DCM. The ratio of Chla at the DCM to that at the surface, integrated Chla and depth of DCM were estimated by forcing the empirical model of Brewin et al. (Submitted, this issue) with climatological monthly averages of CHL within each gyre.

Figure 12. Simulations of SST (a), depth of the DCM (b), surface Chla (averages to top 40m, c) and DCM Chla (d) from the coupled ERSEM-GOTM model (Hardman-Mountford et al.2013) at the centre of the SAG over the period 1997 to 2004.

Figure 13. Seasonal cycles of SST, Gyre Area (GA), CHL and PAR in the NAG from 1998 to 2012. Seasonal cycles were determined from averaging monthly composites of RS data within gyre boundary limits of 0.1 mg m^{-3} (top two figures: a and b) and 0.15 mg m^{-3} (bottom two figures: c and d). The timing of AMT cruises (AMT-5 to AMT-21) are illustrated in the top figure

Figure 14. Seasonal cycles of SST, Gyre Area (GA), CHL and PAR, in the SAG from 1998 to 2012. Seasonal cycles were determined from averaging monthly composites of RS data within gyre boundary limits of 0.1 mg m^{-3} (top two figures: a and b) and 0.15 mg m^{-3} (bottom two figures: c and d). The timing of AMT cruises (AMT-5 to AMT-21) are illustrated in the top figure.

Figure 15.Annual anomalies and trends in the NAG for SST, CHL, GA and PAR, from 1998 to 2012, along with the Multivariate ENSO Index (MEI). Variables were spatially averaged within the NAG (using a 0.15 mg m^{-3} boundary in CHL).

Figure 16. Annual anomalies and trends in the SAG for SST, CHL, GA and PAR, from 1998 to 2012, along with the Multivariate ENSO Index (MEI). Variables were spatially averaged within the SAG (using a 0.15 mg m^{-3} boundary in CHL).

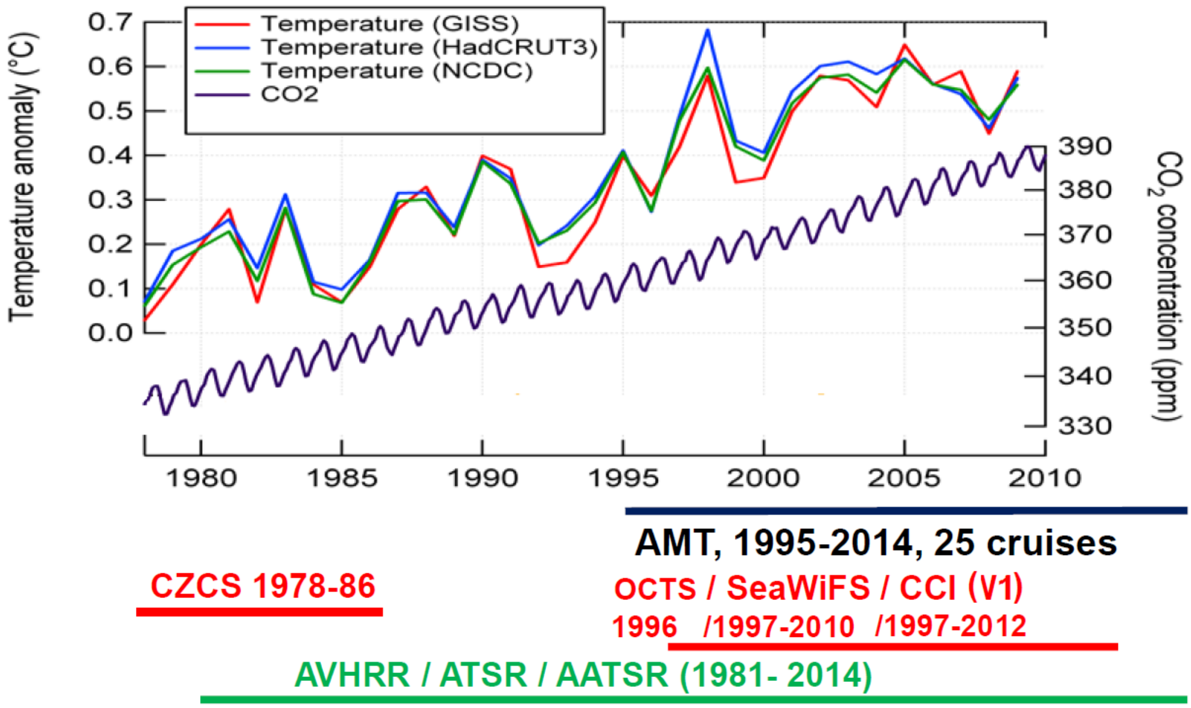

Figure 1. Global temperatures and atmospheric CO2 concentrations from 1978 – 2010 at Mona Loa, Hawaii (Northern hemisphere); time spans of Remote Sensing (RS) data sets and AMT cruises. GISS refers to the analysis by NASA's Goddard Institute for Space Studies; HadCRUT3 refers to the third revision of analysis by the UK Met Office Hadley Centre and Climate Research Unit of the University of East Anglia; and NCDC refers to analysis by NOAA's National Climatic Data Centre. The plot was adapted from https://ourchangingclimate.wordpress.com/2010/04/11/recent-changes-in-the-sun-co2-and-global-average-temperature-little-ice-age-onwards/ (accessed 05/05/15)

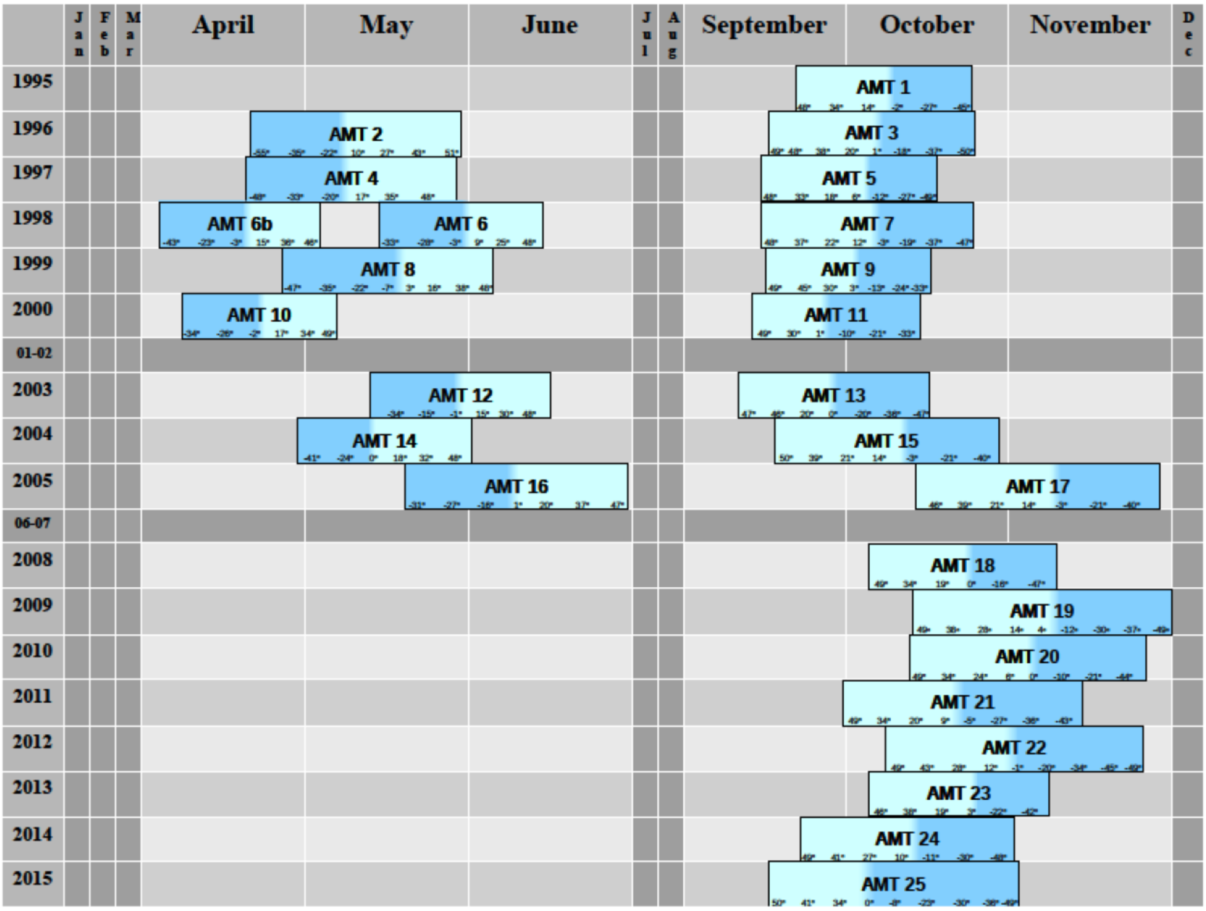

Figure 2. Annual and seasonal coverage of AMT cruises from AMT-1 through to AMT-25 (1995-2015).

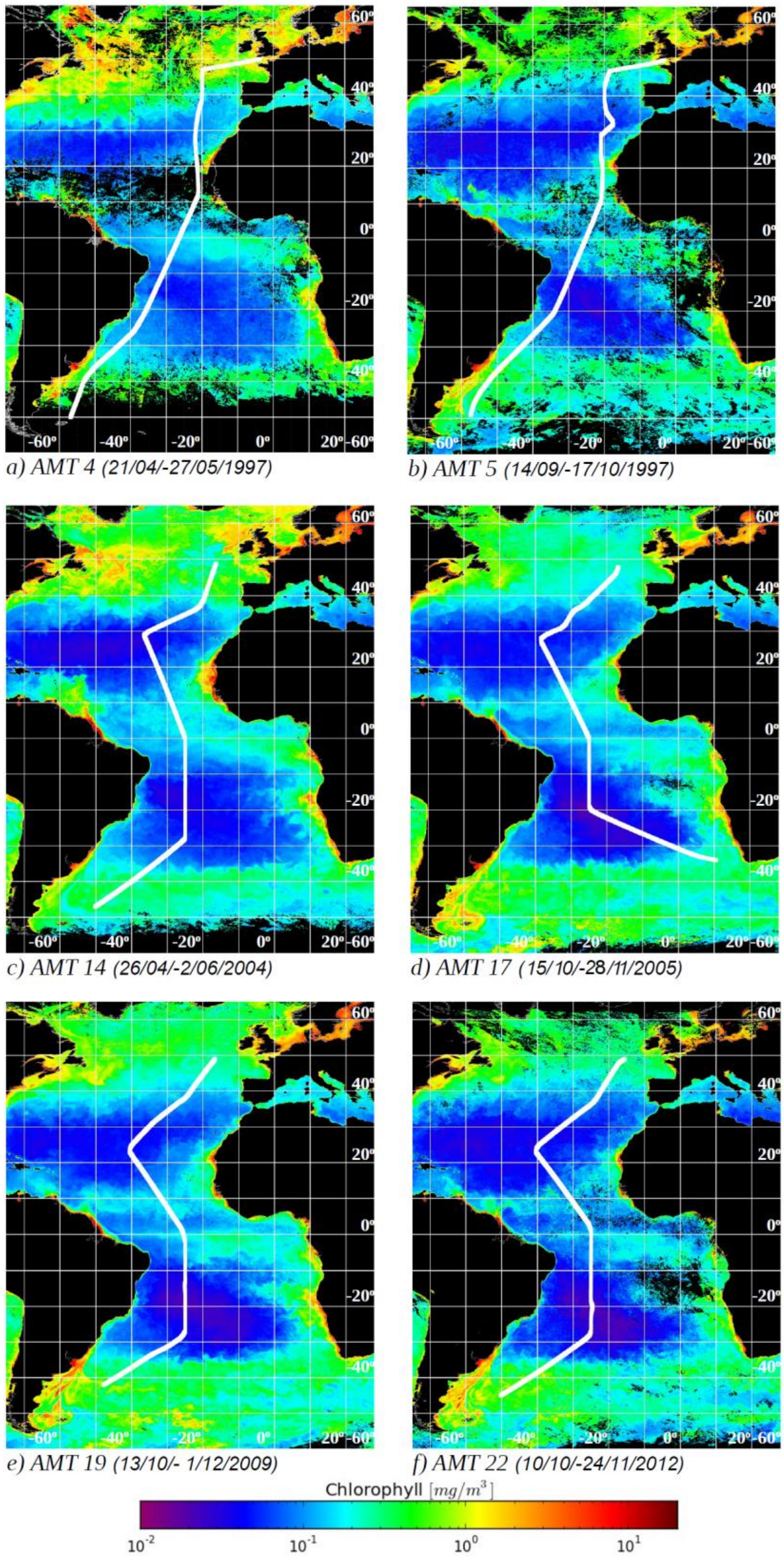

Figure 3. Atlantic CHL composites from OCTS (AMT-4) and OC-CCI (AMT-5 to AMT22) with AMT cruise tracks overlain. Including: AMT-4 (AFBS, 21/04/97 to 27/05/97); AMT-5 (BFAS, 14/09/97 to 17/10/97); AMT-14 (AFBS, 26/04/04 to 2/06/04); AMT-17 (BFAS, 15/10/05 to 28/11/05); AMT-19 (BFAS, 13/10/09 to 1/12/09); and AMT-22 (BFAS, 10/10/12 to 24/11/12).

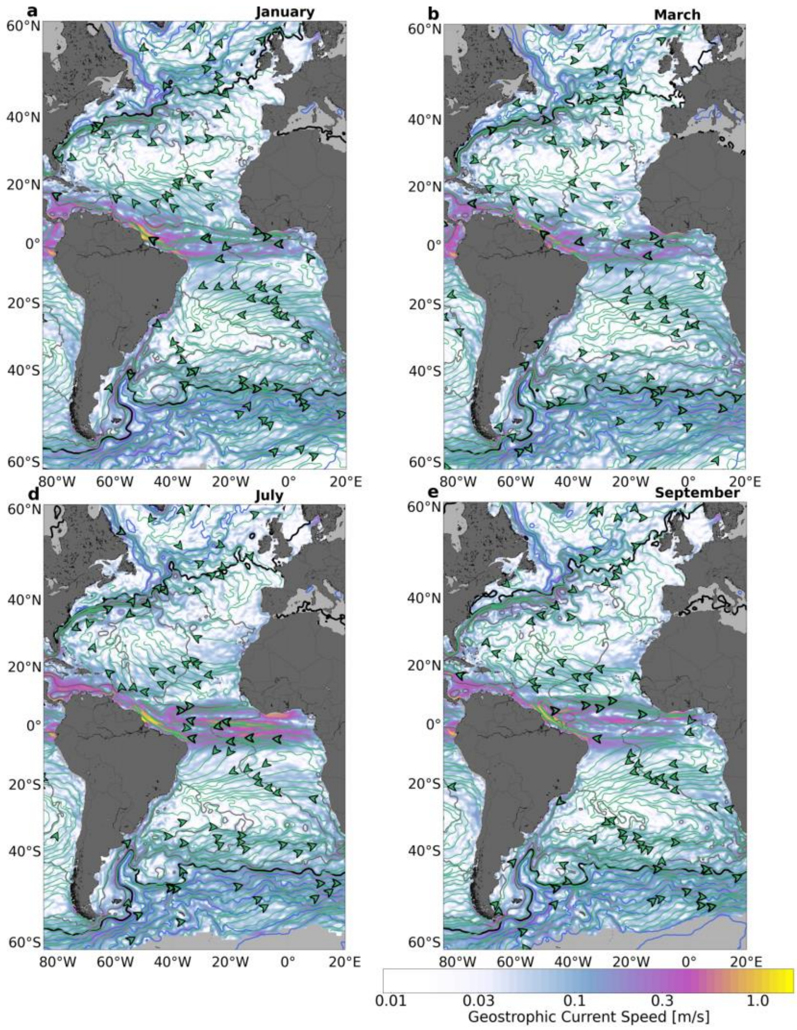

Figure 4. Monthly climatology of sea-surface height (SSH) and surface-geostrophic-current derived from AVISO altimetry data for the Atlantic Ocean for: a) January; b) March; c) May; d) July; e) September; and f) November. The magnitude speed (background shading on a log scale) is overlaid with SSH contours at 0.2 m intervals. Grey (blue) contours show regions of positive (negative) SSH, with the zero SSH line shown in black. Current direction is shown in the green, arrow-annotated, streamlines.

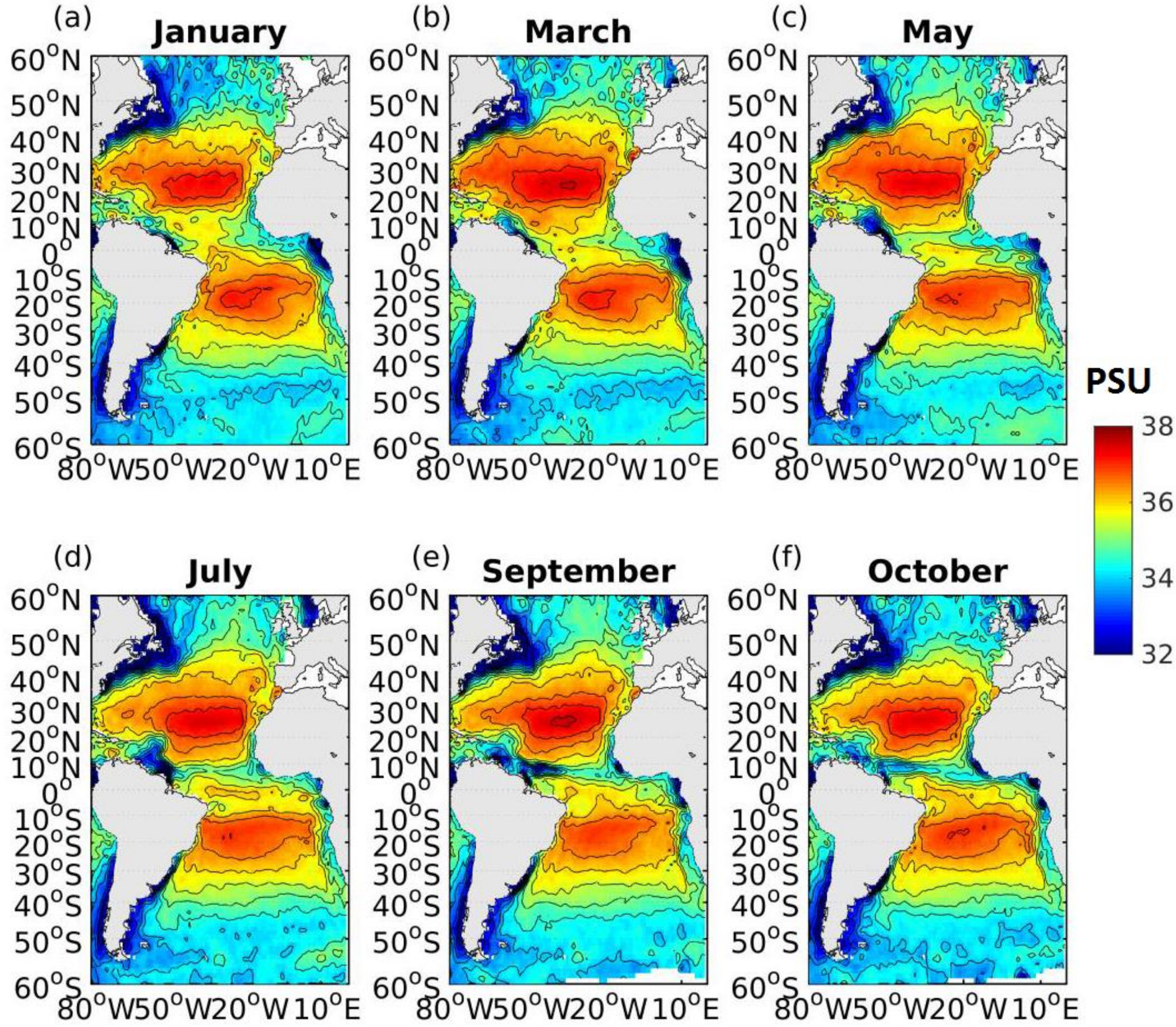

Figure 5. The monthly composites of Sea Surface Salinity (SSS), derived from SMOS in the Atlantic Ocean for: a) January; b) March; c) May; d) July; e) September; and f) October.

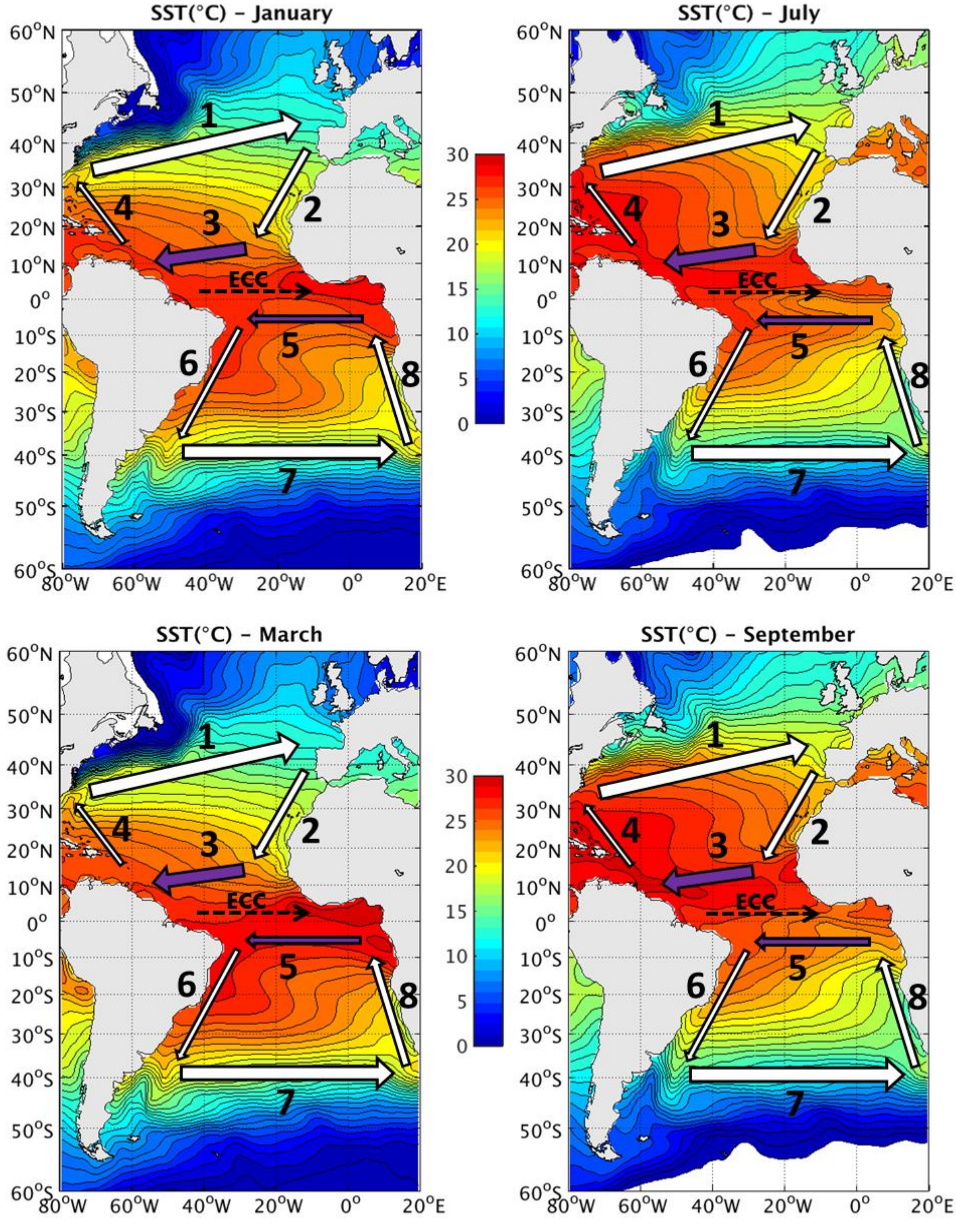

Figure 6. Monthly climatology of Sea Surface Temperature, derived from OISST data, for January, July, March and September, with a schematic of main current systems overlain, including: 1 = North Atlantic Current (NAC); 2 = Canaries Current (CC); 3 = North Equatorial Current (NEC); 4 = Antilles Current (AntC); 5 = South Equatorial Current (SEC); 6 = Brazil Current (BC); 7 = South Atlantic Current (SAC); and 8 = Benguela Current (BenC). Breadth of arrows represents strength of flow with purple infill for low salinity currents.

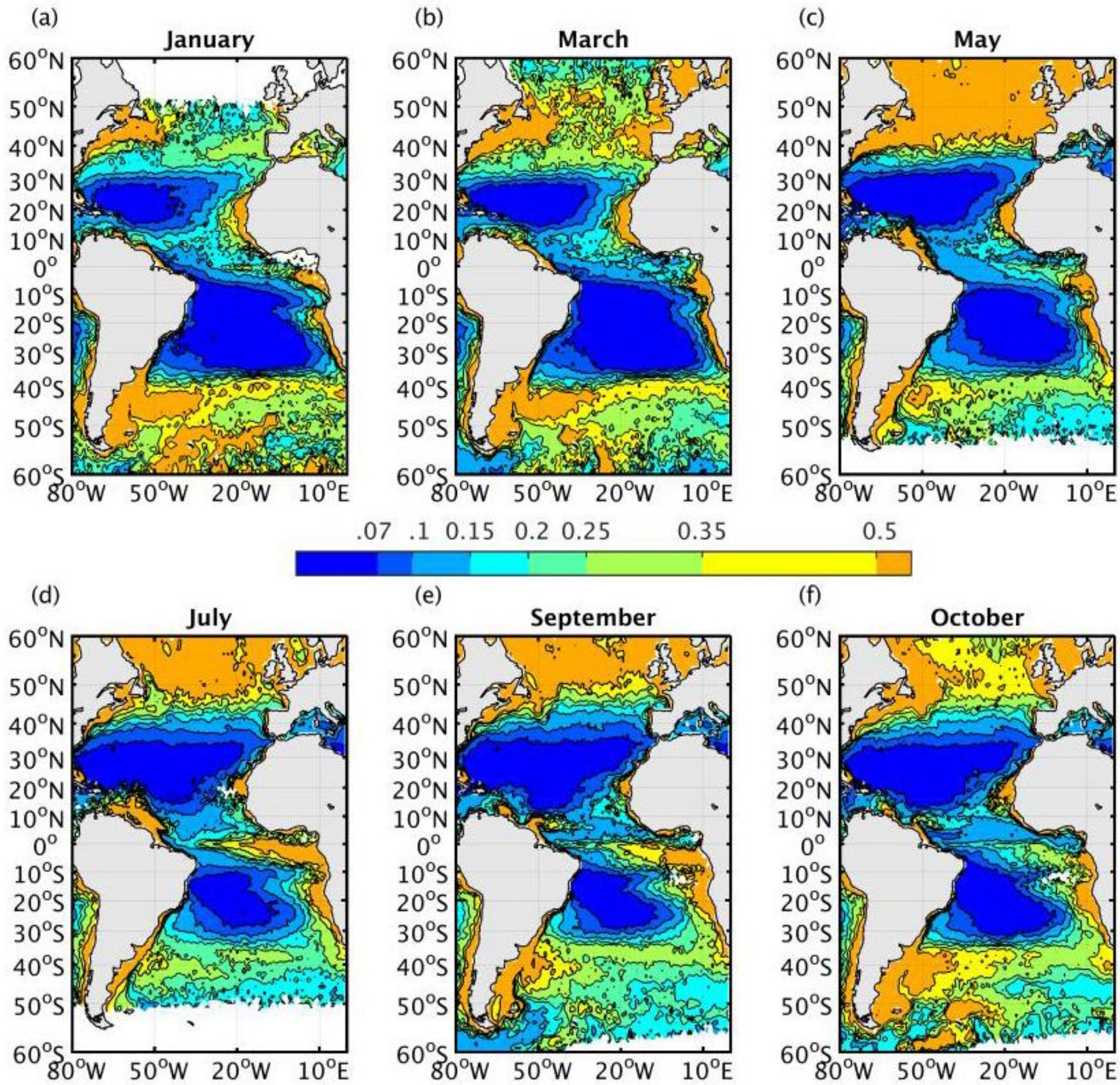

Figure 7. Monthly climatology of CHL (OC-CCI data 14y composite) in the Atlantic Ocean for: a) January; b) March; c) May; d) July; e) September; and f) October.

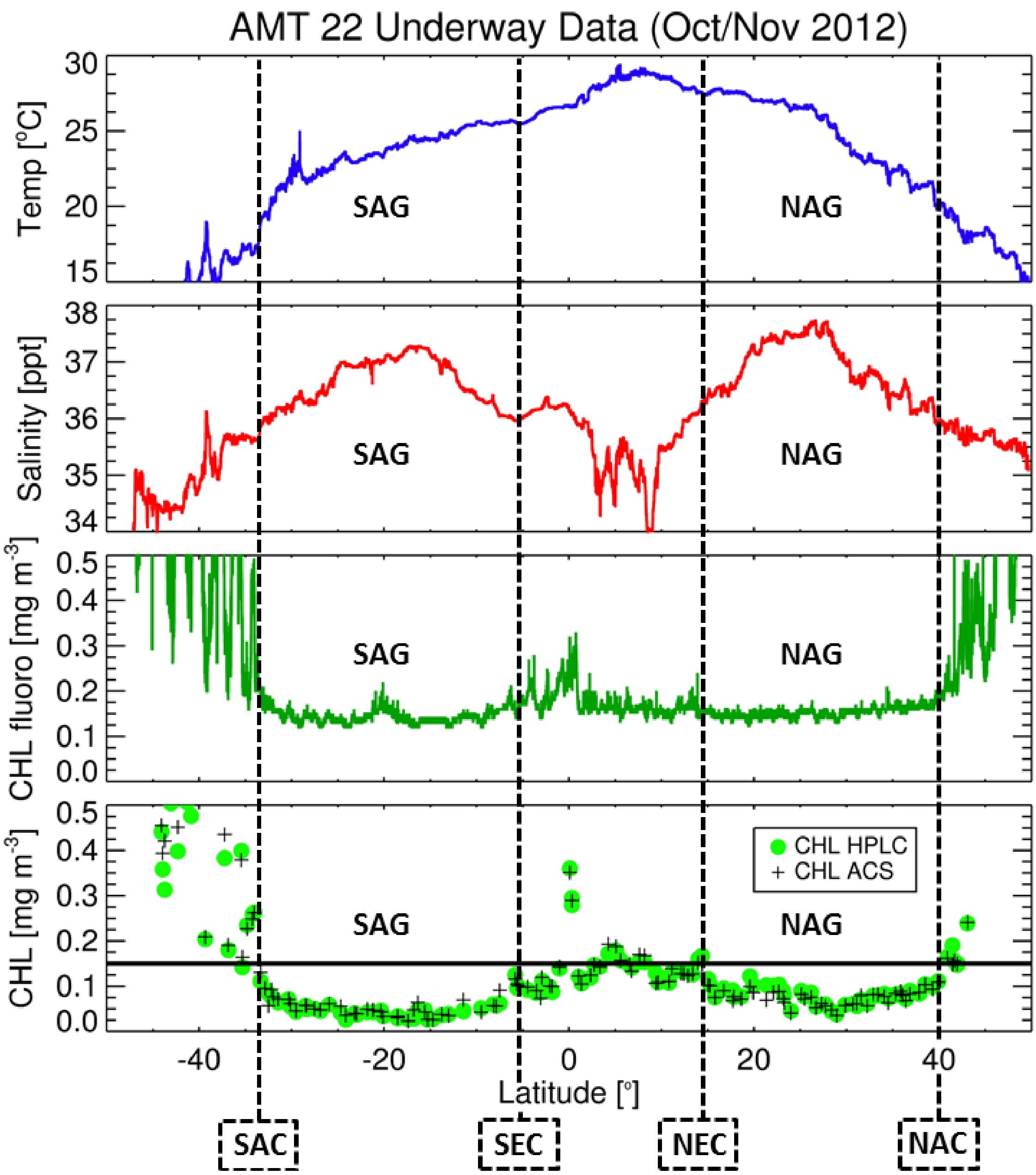

Figure 8. Along-track AMT-22 data on: surface temperature (SST, denoted Temp in the figure); Salinity (SSS); surface Chla fluorescence (CHL); and surface Chla (CHL) derived from HPLC from discrete surface water samples taken along-track, and from measurements from an ACS. Measurements are from pumped surface-layer water (nominally 5 m depth) measured continuously by shipboard instruments, illustrating the sharp change of all variables at the gyre edges. Dashed lines show the approximate locations of the gyres edges (North Atlantic Gyre (NAG) and South Atlantic Gyre (SAG)), the South Atlantic Current (SAC), South Equatorial Current (SEC), North Equatorial Current (NEC) and North Atlantic Current (NAC) regions of NAG and SAG. Black horizontal line on the bottom plot shows the 0.15 mg m-3 CHL boundary.

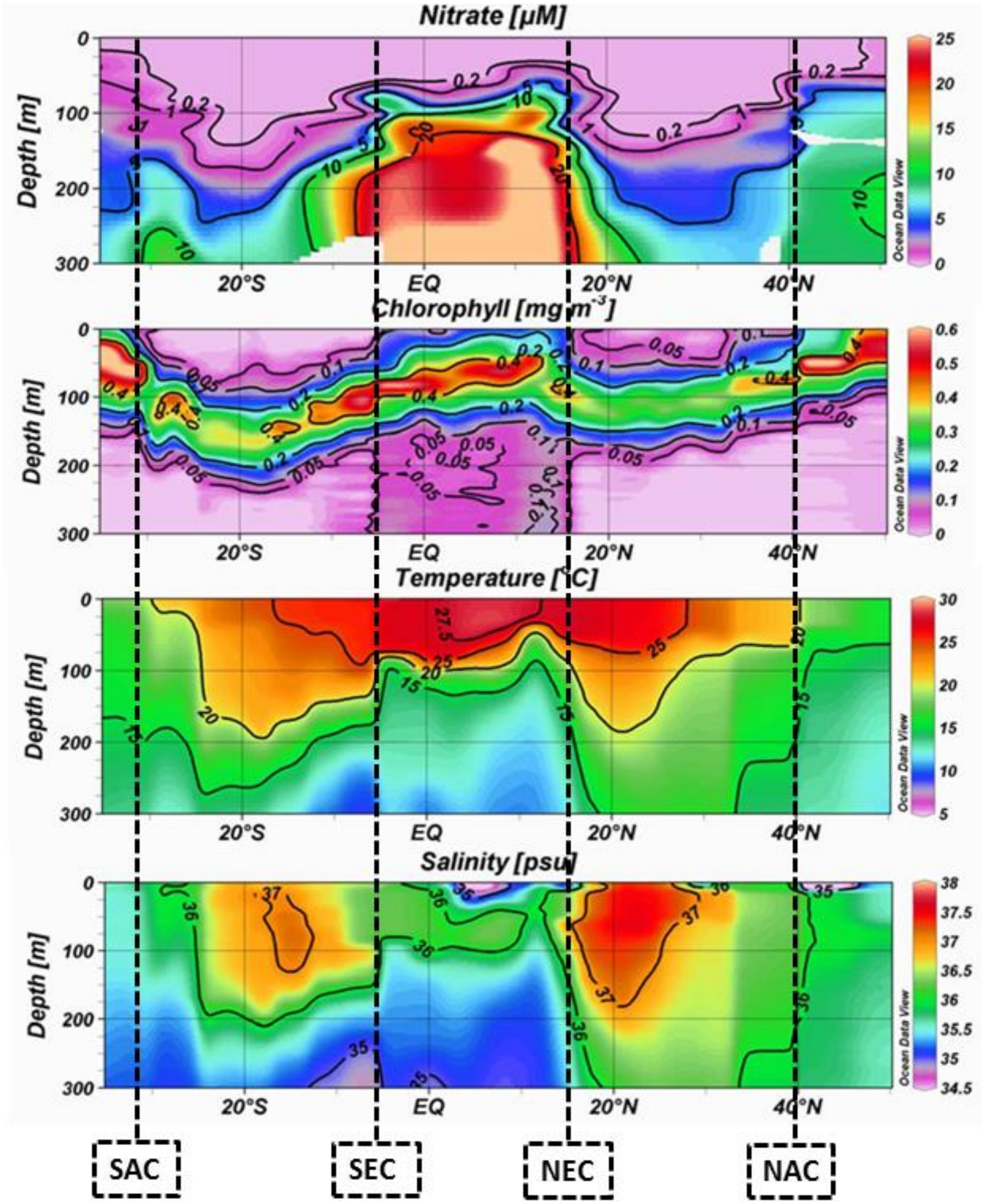

Figure 9. Contoured cross-sections of Nitrate, Chla, Temp, Salinity for AMT-17, with the approximate locations of the South Atlantic Current (SAC), South Equatorial Current (SEC), North Equatorial Current (NEC) and North Atlantic Current (NAC). Figures were adapted from AMT cruise report 17, available at http://www.amt-uk.org/pdf/AMT17_report.pdf.

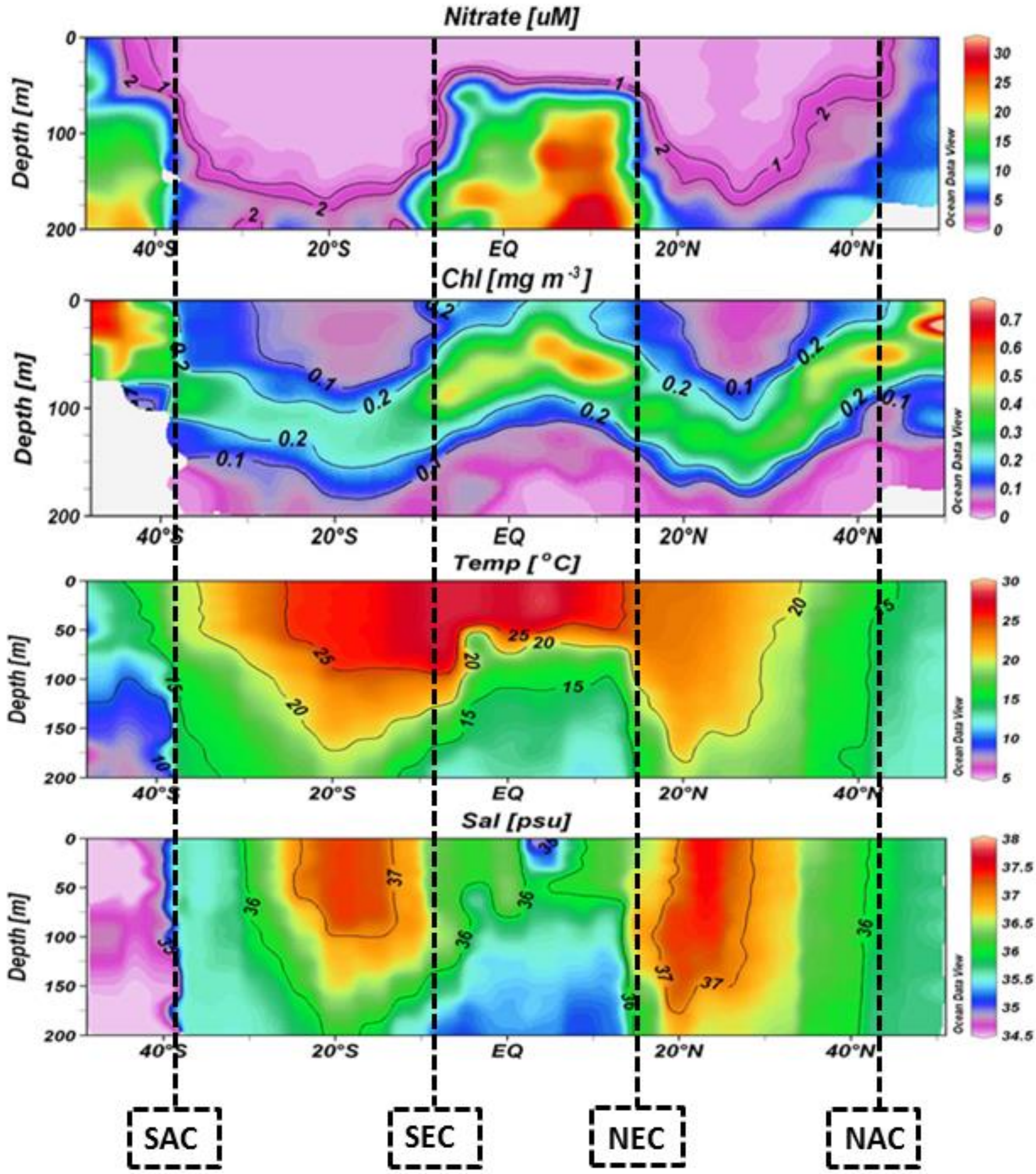

Figure 10. Contoured cross-sections of Nitrate, Chla, Temp, Salinity for AMT-14, with the approximate locations of the South Atlantic Current (SAC), South Equatorial Current (SEC), North Equatorial Current (NEC) and North Atlantic Current (NAC). Figures were adapted from AMT cruise report 14, available at http://www.amt-uk.org/pdf/AMT14_report.pdf.

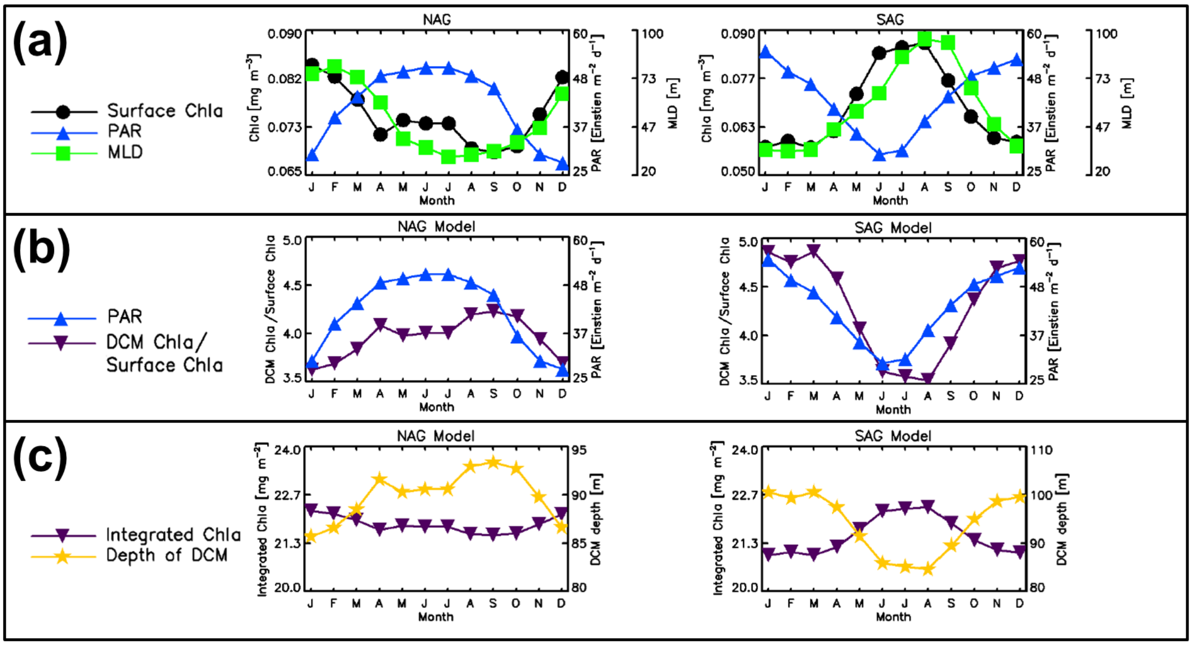

Figure 11. (a) Shows RS climatological monthly averages of surface Chla (CHL) and PAR, and average mixed-layer depth, all averaged within each gyre (using a 0.15 mg m^{-3} boundary in CHL). (b) Shows seasonal cycles in estimates of the ratio of Chla at the DCM to that at the surface together with climatological monthly averages of PAR, and (c) shows seasonal cycles integrated Chla (vertically integrated within 1.5 times the euphotic depth) and depth of DCM. The ratio of Chla at the DCM to that at the surface, integrated Chla and depth of DCM were estimated by forcing the empirical model of Brewin et al. (Submitted, this issue) with climatological monthly averages of CHL within each gyre.

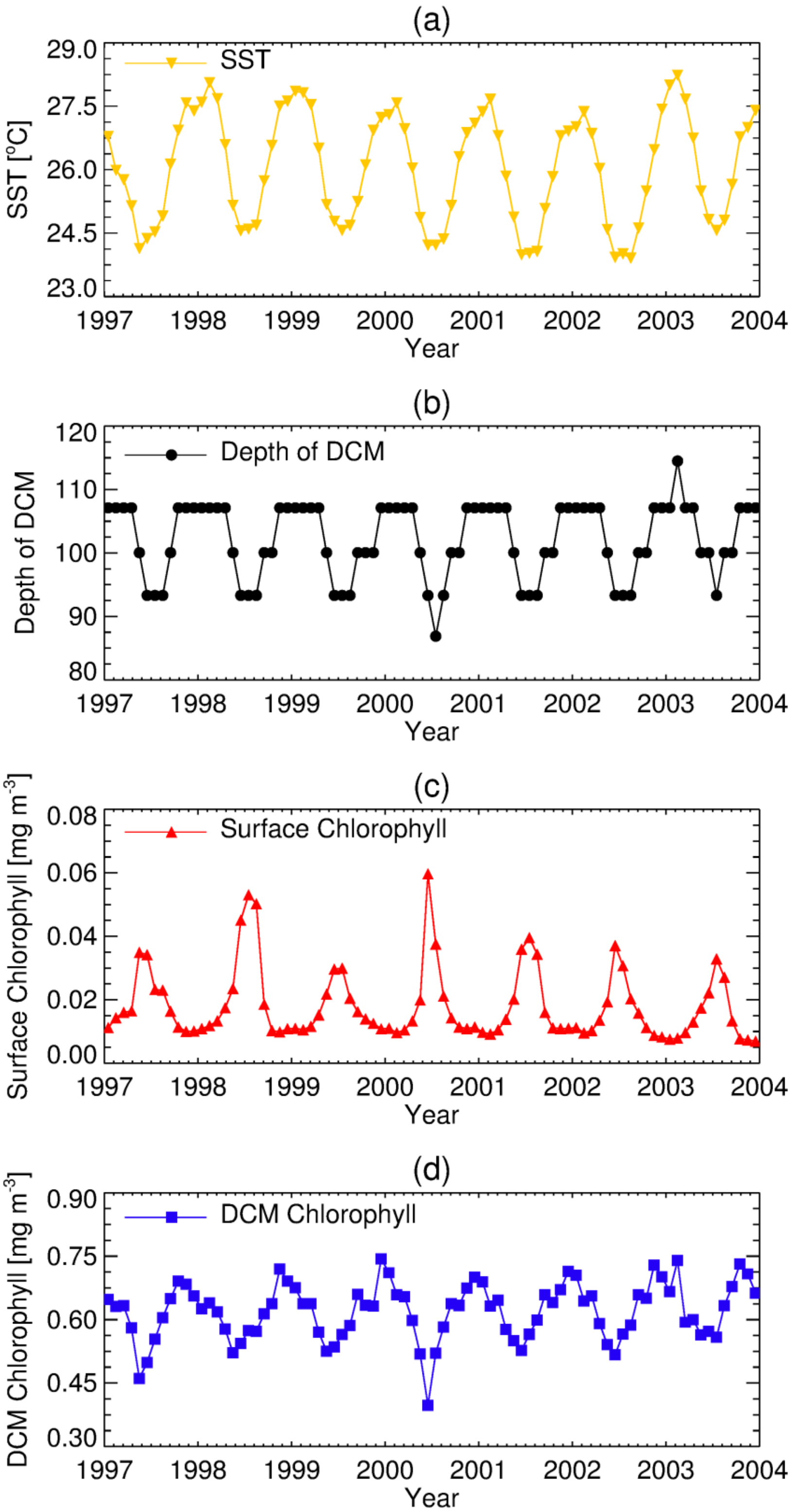

Figure 12. Simulations of SST (a), depth of the DCM (b), surface Chla (averages to top 40m, c) and DCM Chla (d) from the coupled ERSEM-GOTM model (Hardman-Mountford et al. 2013) at the centre of the SAG over the period 1997 to 2004.

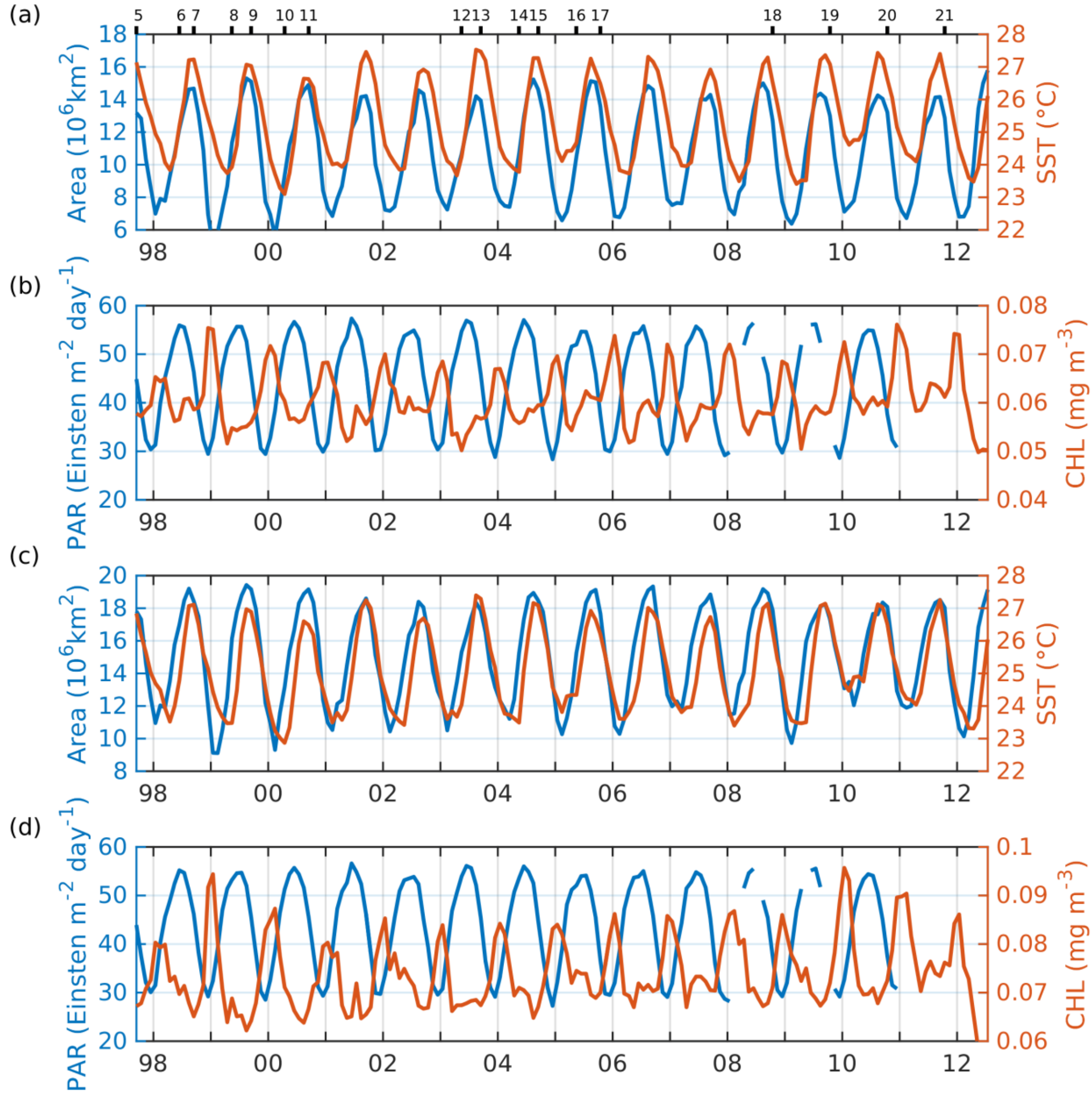

Figure 13. Seasonal cycles of SST, Gyre Area (GA), CHL and PAR in the NAG from 1998 to 2012. Seasonal cycles were determined from averaging monthly composites of RS data within gyre boundary limits of 0.1 mg m^{-3} (top two figures: a and b) and 0.15 mg m^{-3} (bottom two figures: c and d). The timing of AMT cruises AMT-5 to AMT-21 are illustrated in the top figure.

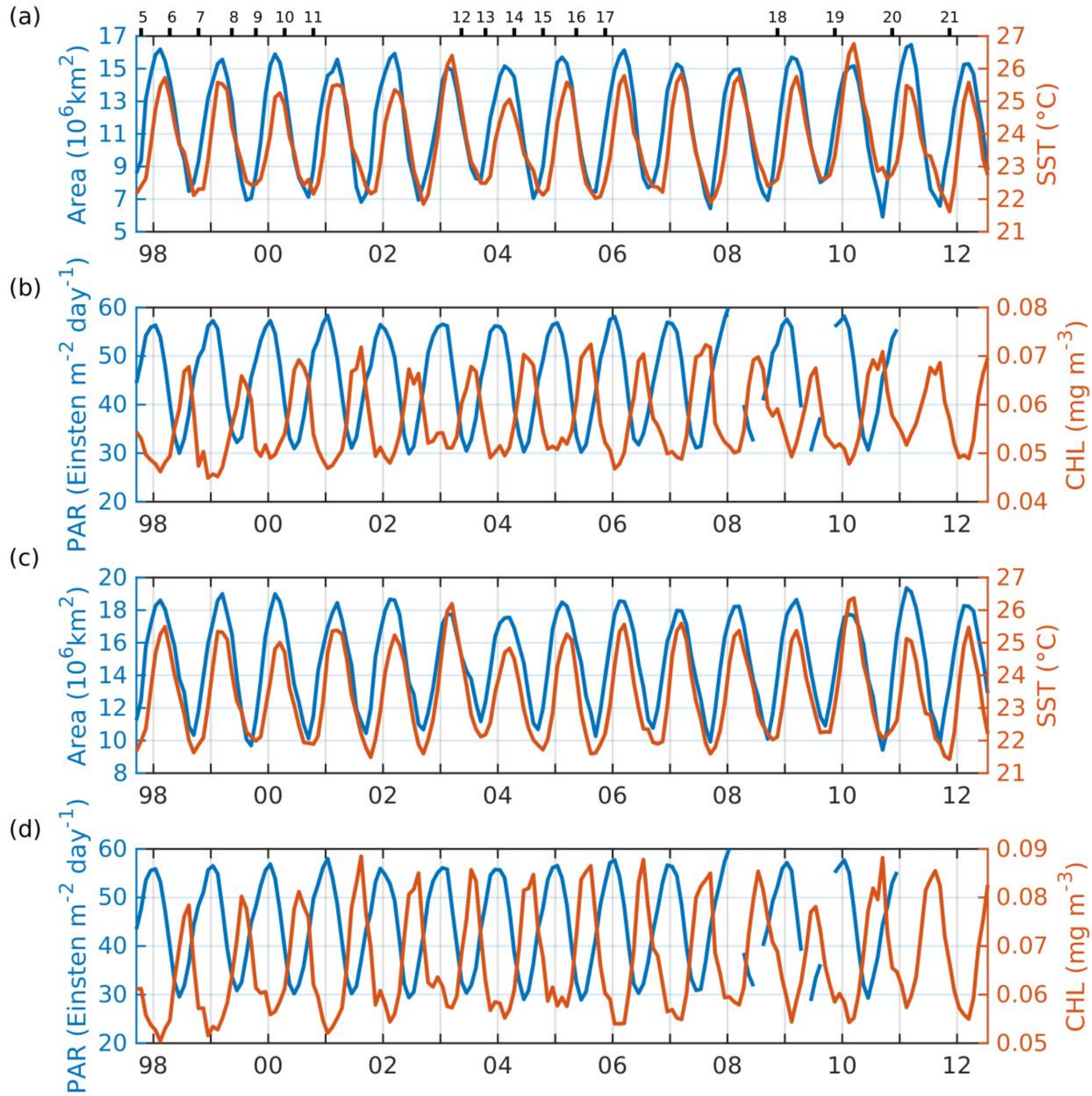

Figure 14. Seasonal cycles of SST, Gyre Area (GA), CHL and PAR, in the SAG from 1998 to 2012. Seasonal cycles were determined from averaging monthly composites of RS data within gyre boundary limits of 0.1 mg m^{-3} (top two figures: a and b) and 0.15 mg m^{-3} (bottom two figures: c and d). The timing of AMT cruises AMT-5 to AMT-21 are illustrated in the top figure.

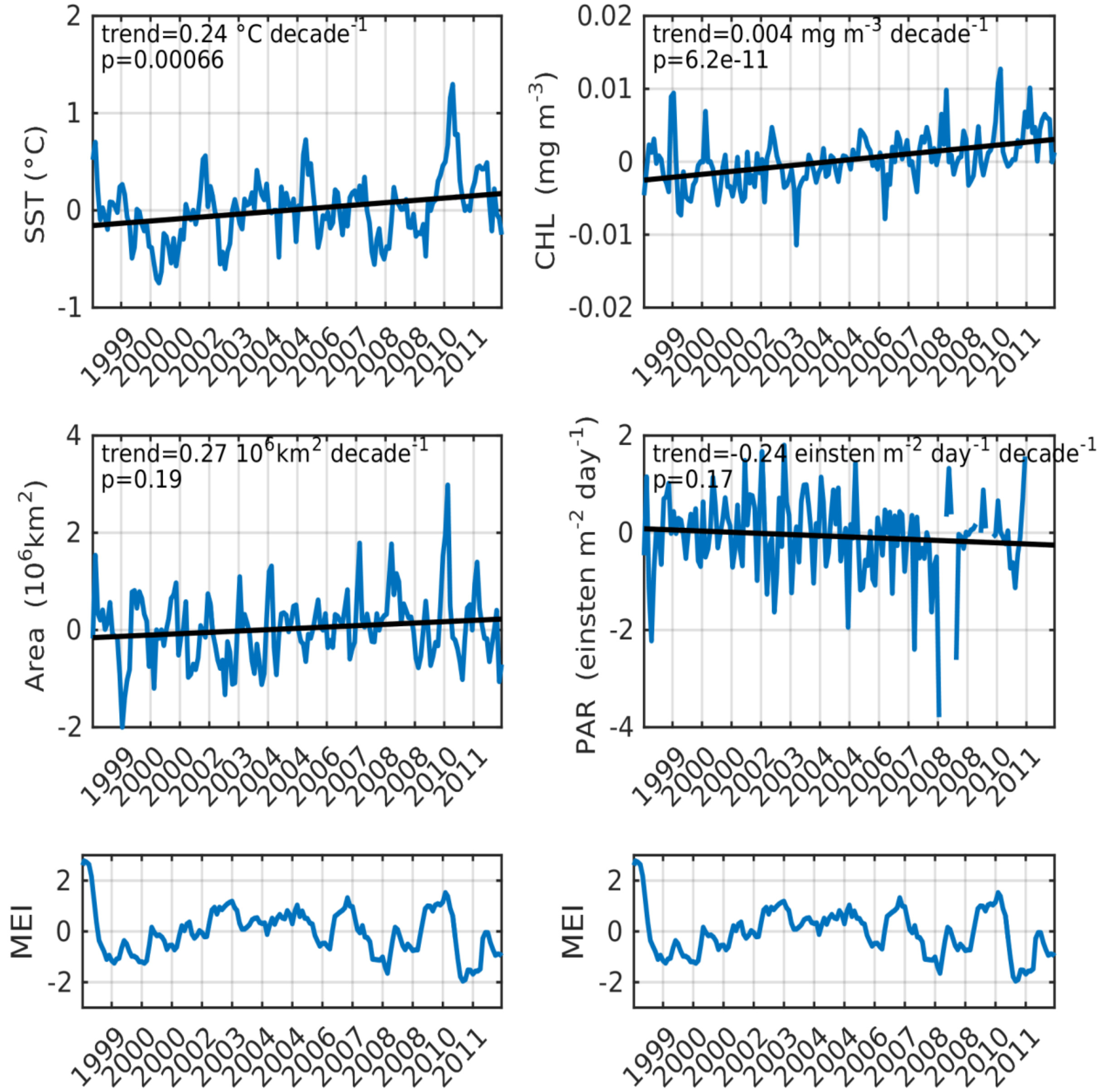

Figure 15.Annual anomalies and trends in the NAG for SST, CHL, GA and PAR, from 1998 to 2012, along with the Multivariate ENSO Index (MEI). Variables were spatially averaged within the NAG (using a 0.15 mg m^{-3} boundary in CHL).

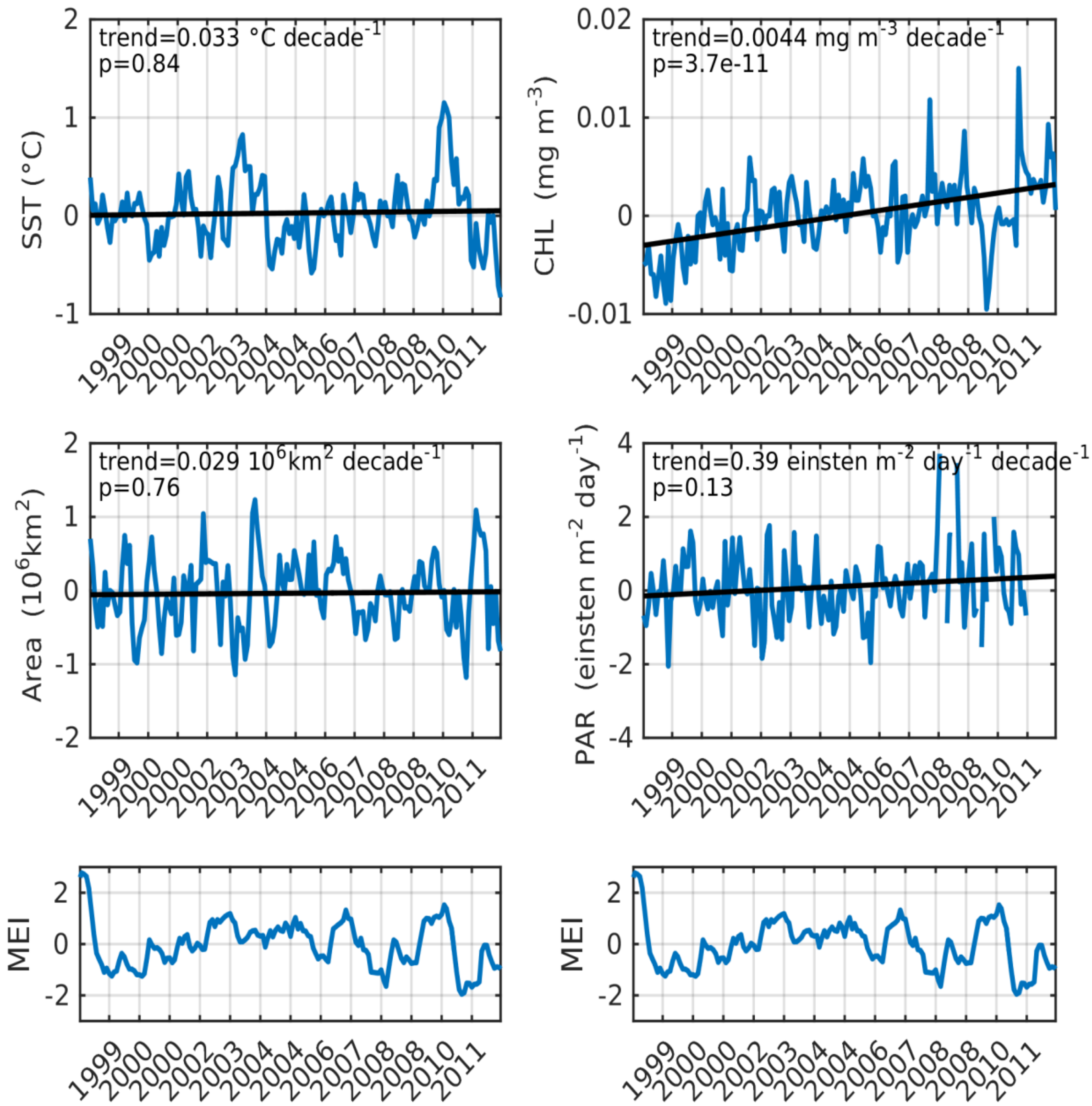

Figure 16. Annual anomalies and trends in the SAG for SST, CHL, GA and PAR, from 1998 to 2012, along with the Multivariate ENSO Index (MEI). Variables were spatially averaged within the SAG (using a 0.15 mg m^{-3} boundary in CHL).